Journal of Environmental Chemical Engineering 10 (2022) 108143

Contents lists available at ScienceDirect

Journal of Environmental Chemical Engineering

journal homepage: www.elsevier.com/locate/jece

Performance and modeling of Ni(II) adsorption from low concentrated wastewater on carbon microspheres prepared from tangerine peels by $FeCl_3$-assisted hydrothermal carbonization

Jose L. Diaz De Tuesta [a,*], Fernanda F. Roman [a,b,c], Vitor C. Marques [a,d], Adriano S. Silva [a,b,c], Ana P.F. Silva [a], Tatiane C. Bosco [d], Assem A. Shinibekova [a,e], Sadenova Aknur [a,e], Marzhan S. Kalmakhanova [e], Bakytgul K. Massalimova [e], Margarida Arrobas [a], Adrián M. T. Silva [b,c], Helder T. Gomes [a]

[a] Centro de Investigação de Montanha (CIMO), Instituto Politécnico de Bragança, Campus de Santa Apolónia, 5300-253 Bragança, Portugal
[b] Laboratory of Separation and Reaction Engineering - Laboratory of Catalysis and Materials (LSRE-LCM), Faculdade de Engenharia, Universidade do Porto, Rua Dr. Roberto Frias, 4200-465 Porto, Portugal
[c] ALiCE—Associate Laboratory in Chemical Engineering, Faculdade de Engenharia, Universidade do Porto, 4200-465 Porto, Portugal
[d] Universidade Tecnológica Federal do Paraná (UTFPR), Campus de Ponta Grossa, Rua Doutor Washington Subtil Chueire, 330 Jardim Carvalho, 84017-220 Londrina PR, Brazil
[e] M.Kh. Dulaty Taraz Regional University, Taraz. Department of Chemistry and Chemical Engineering, Taraz 080012, Kazakhstan

ARTICLE INFO

Editor: Fumitake Takahashi

Keywords:
Heavy metal
Carbonaceous material
Citric peels
Waste valorization
Wastewater treatment
Nonlinear
Error function
Circular economy

ABSTRACT

The presence of heavy metals in the environment as a consequence of human activity is an issue that has caught the attention of researchers to find wastewater treatment solutions, such as adsorption. In this work, hydrochars and activated carbon microspheres are prepared from tangerine peels as carbon precursor and $FeCl_3$ as activating and structure-directing agent in the hydrothermal carbonization, allowing to obtain hydrochar microspheres ranging from 50 to 3615 nm. In addition, a pyrochar was prepared by pyrolysis of the same precursor. The activated carbon shows the highest surface area (S_{BET} up to 287 $m^2\ g^{-1}$), but the basicity of the pyrochar (1.83 mmol g^{-1}, S_{BET} = 104 $m^2\ g^{-1}$) was determinant in the adsorption of Ni, being considered the carbon-based material with the highest uptake capacity of Ni. Isotherm and kinetic adsorption of Ni on the most representative activated carbon microsphere, pyrochar and hydrochar microsphere are assessed by 10 and 7 models, respectively.

1. Introduction

Heavy metals are natural elements presenting high atomic mass and density (> 5 g cm^{-3}). Some of these metals are essential for animals, with indispensable functions for human metabolism [62]. However, several studies indicate that some heavy metals are likely to be carcinogenic (hexavalent chromium, arsenic, cobalt, nickel, antimony, vanadium and mercury), mutagenic (arsenic and vanadium), teratogenic (arsenic), allergenic (nickel) or endocrine-disrupting (silver, copper, zinc and selenium). Low levels of nickel result in reduced growth in intrauterine development, and its deficiency can reduce iron absorption, leading to anemia [51]. The main adverse effects caused by exposure to compounds containing this metal are skin allergies, lung fibrosis and lung cancer, depending on their ability to enter cells [10,98]. Despite its effects, nickel(II) is largely used in the manufacturing process of stainless steel, metallic alloys and batteries [80]. The release of this metal into the environment may occur from various industries, *viz.,* nickel plating, zinc-based casting industry and storage batteries, silver refinery, mining and metallurgy of nickel [5,39].

The presence of nickel in drinking water can also occur due to corrosion of pipes containing nickel in their composition or even to the poor removal of this metal by water treatment systems [60]. Regulatory environmental agencies establish concentration limits for nickel, owing to the risks presented by its existence in drinking water and wastewater. For instance, the World Health Organization establishes as a guideline a value of 0.07 mg L^{-1} for the concentration of nickel in drinking waters

* Corresponding author.
E-mail address: jl.diazdetuesta@ipb.pt (J.L. Diaz De Tuesta).

https://doi.org/10.1016/j.jece.2022.108143
Received 9 February 2022; Received in revised form 3 June 2022; Accepted 20 June 2022
Available online 22 June 2022

(WHO/SDE/WSH/07.08/55). The concentration of nickel may range from 0.5 mg L^{-1} to 192 mg L^{-1} in wastewater effluents [53]. Adsorption on several carbon-based adsorbents [80,95,96] has resulted in efficient processes for the removal of Ni. However, many studies report high uptake capacities, since the removal of Ni from waste waters is normally studied considering high loads of the heavy metal (> 50 mg L^{-1}) [24,53,59]. The feasibility of the adsorption of nickel on carbonaceous adsorbents should also be explored at low nickel concentrations.

An efficient scenario allowing to decrease the costs of the adsorption process and to reach a circular economy approach consists in the development of technologies to valorize wastes by their transformation into suitable adsorbents [25,84,89]. In this sense, the scientific community has been putting a great effort into the development of carbon-based adsorbents from biomass wastes coming from agro-industrial activities, such as fruit peels [25], shell of nuts [42], bagasses [16], among others. By using biomass waste as a carbon precursor, different carbon-based adsorbents can be obtained, *viz.* pyrochars, hydrochars, or activated carbons, depending on the carbonization processes applied [16]. A pyrochar (PC) is obtained through the thermal treatment of the precursor at 400–1000 ºC in an inert or oxygen-limited environment [97]. Hydrochars (HCs) can be prepared by hydrothermal carbonization (HTC), which consists in a thermochemical conversion in the presence of water at temperatures ranging from 150 to 350 ºC and autogenous pressure [71]. HTC is interesting because of its technical simplicity, low cost and energy efficiency. Activated carbons (ACs) are typically obtained through two steps: activation and carbonization. Activation can be conducted using chemical (treatment of the precursor with oxidants) or physical (steam, CO_2 and air) methods [94]. As an activation step, HTC also works as an efficient process to obtain a suitable precursor (HCs) for the production of ACs [16].

The chemical activation to prepare ACs from biomass waste has been studied with different activating agents, such as inorganic acids, bases or salts [2,94]. However, there are scarce studies on HTC of biomass wastes using additives to improve the physicochemical properties of the resultant HCs [16,66,71,85]. The use of chemical agents in HTC can be exploited to introduce improved surface chemistry for adsorption applications of the resultant HCs or ACs. Furthermore, chemical agents in HTC can also act as structure-directing agents to prepare carbonaceous spheres [9]. Among them, iron (III) chloride has proved to be an excellent activating agent for the preparation of carbonaceous materials [3,55,81] and as a metal doping for the adsorption of heavy metals from aqueous solution [11,27,53]. In fact, for carbonaceous adsorbents, the metals and functional groups on their surfaces, with acid or base character, play an important role in the adsorption process [80]. In this sense, HCs are rich in functional groups that can greatly improve chemical reactivity [36]. Because of this, many scientists have been testing HCs as adsorbents for the removal of heavy metals, pesticides, and drug residues [35]. However, the influence of the adsorbent's characteristics (*e.g.* functionalities, morphology, or textural properties) on the adsorption of Ni has not been deeply studied so far.

The properties of the carbon-based materials not only depend on the type and operating conditions of the carbonization process but also on the carbon precursor selected for their preparation. The materials obtained under the same conditions can present significant differences in their characteristics when other carbon precursors are used [16]. Therefore, the biomass waste used for the preparation of adsorbents should be carefully selected. In this sense, citrus fruit peels have shown to be efficient precursors for preparing carbon-based materials [23,25]. As the precursor contains citric acid, interesting carbon-based materials may be obtained, since citric acid is used as catalyst to develop this type of material [85,87].

Citrus fruits are one of the largest fruit crops in the world. Similarly, the citrus industry is also the second largest fruit processing industry, surpassed only by the grape industry, which mainly produces wine [38]. Approximately one-third of the citrus fruits are processed for juice production, resulting in 50–60 % of organic waste, typically constituted by the peel, seeds and leaf residues [75]. It is noteworthy that due to the amount of organic matter present in citrus fruit peels, the disposal of this type of residue directly in the soil can cause damage, given its ability to change the physicochemical characteristics of the soil [79]. Currently, land space occupation and pollution with phenolic compounds due to dumping of waste are becoming problematic [26]. For this reason, the development of techniques to valorize the large amount of waste generated in the citrus juice processing industry is required. In this sense, the production of biochars from diverse citrus peels has become interesting as a low-cost alternative to obtain high-value products, avoiding the pollution of waste dumping [65,78,81,83].

This work deals with the preparation of activated carbon, pyrochar and hydrochar materials using tangerine peels as carbon precursor and their assessment in the removal of Ni(II) by adsorption. Hydrochars (HCs) are prepared by HTC assisted with $FeCl_3$, known as a catalyst of carbonization processes [55] and later used as a precursor for the preparation of activated carbons (ACs) by pyrolysis at the same conditions of pyrochar (PC) directly prepared from the tangerine peels. The different properties of the ACs, PC and HCs and how they affect the adsorption of Ni(II) are analyzed, and the kinetic and equilibrium adsorption of Ni(II) on them is modeled. To the best of our knowledge, there is a scarcity of studies dealing with the valorization of tangerine peels, as is the case of other peels, especially considering $FeCl_3$-assisted HTC. Similarly, few studies assess ACs, PCs and HCs prepared from the same source to be applied to the adsorption of a heavy metal at similar operating conditions.

2. Description of adsorption models

The modelling of the adsorption process is invaluable, not only for the prediction of the solute adsorption onto the adsorbent at different operating conditions, but also for a better understanding of the adsorption mechanism occurring on a system [20,28]. Adsorption isotherms data (quantification of adsorbed solute per unit mass of adsorbent at a constant temperature for different solute concentrations in solution at the equilibrium) can be processed for a deep understanding of the interaction between the solute (Ni(II) in this work) and the adsorbent. The constants obtained from the different models provide important information on the affinities of the adsorbent for the removal of the pollutant and on the mechanisms of adsorption. The application of kinetic adsorption is also useful in studying the dynamics of the adsorption mechanism in terms of the order of the adsorption rate constant. Additionally, the parameters obtained as results of the fitting kinetic models allow to assess the time required to remove Ni(II) on the selected adsorbent [49,76].

2.1. Equilibrium isotherm adsorption models

2.1.1. Two-parameter models

The Langmuir equation is a well-known isotherm model that assumes that adsorption occurs on a homogeneous surface of an adsorbent containing sites that are equally available for adsorption [52]. The separation factor (R_L) is an important parameter of the Langmuir isotherm typically used to verify whether the adsorption under study is unfavourable ($R_L > 1$), linear ($R_L = 1$), favourable ($0 < R_L < 1$) or irreversible ($R_L = 0$). Langmuir equation and R_L are expressed by Eqs. (1–2),

$$q_e = \frac{q_m \cdot K \cdot C_e}{1 + K \cdot C_e}, \tag{1}$$

$$R_L = \frac{1}{1 + K \cdot C_0}, \tag{2}$$

where q_e and C_e refer to the solute adsorbed per mass of adsorbent (mg g^{-1}) and adsorbate concentration in aqueous media (mg L^{-1}) at equilibria stage, q_m and K are constants (two-parameter model) measured in

mg g^{-1} and L mg^{-1}, respectively, R_L is the separation factor (dimensionless quantity) and C_0 is the initial concentration of the adsorbate.

Freundlich isotherm is an empirical equation (Eq.(3)) widely applied for heterogeneous systems with interaction between the adsorbate, representing suitably non-asymptotic adsorption curves between uptake capacity (q_e) and equilibria concentration (C_e) in the aqueous media [69]. The heterogeneity factor (n) can be employed to indicate if the adsorption is linear, chemical or a physical adsorption process ($n = 1$, $n < 1$ *or* $n > 1$, respectively). This two-parameter model is represented by Eq. (3),

$$q_e = K \cdot C_e^{1/n}, \tag{3}$$

where K is the constant of Freundlich measured in $L^{1/n}$ $mg^{-1/n}$ and n is the exponent.

2.1.2. Three-parameter models

The Sips isotherm model (Eq. (4)) is a combination of the Langmuir and Freundlich isotherms [82]. At high adsorbate concentrations, the equation provides the adsorption capacity in the monolayer, typical of the Langmuir isotherm. At low adsorbate concentrations, the Sips equation is reduced to the Freundlich equation. In the literature, it is possible to find the Sips model named as Koble-Corrigan model [28,77, 93], but Koble and Corrigan used the Sips model indeed, as they described [46]. For this reason, the Koble-Corrigan model was not object of study in this work. This three-parameter model is represented by Eq. (4),

$$q_e = \frac{q_m \cdot K \cdot {C_e}^n}{1 + K \cdot {C_e}^n}, \tag{4}$$

where q_m and K are constants measured in mg g^{-1} and L^n mg^{-n}, respectively, and n is an exponent (three-parameter model).

To improve the fitting of Langmuir and Freundlich equations, Redlich and Peterson developed their model [68], which is mathematically equal to the Radke and Prausnitz isotherm model developed in the adsorption of solutes from dilute aqueous solutions on activated carbon [20,67]. Redlich and Peterson isotherm model is typically expressed as Eq. (5),

$$q_e = \frac{A \cdot C_e}{1 + K \cdot {C_e}^n}, \tag{5}$$

where A and K are constants measured in L mg^{-1} and L^n mg^{-n}, respectively, and n is an exponent.

The General Isotherm Equation (GIE) proposed by Tóth for all types of isotherms was developed to consider the heterogeneity, and the lateral and vertical interaction energies of the adsorbed molecules. The Tóth isotherm model usually applied in the modelling of adsorption systems for the wastewater treatment is the solution of the GIE when the dynamic equilibrium adsorption is higher for the monolayer than the subsequently formed layers [88] and it is expressed by Eq. (6),

$$q_e = \frac{q_m \cdot C_e}{\left(1/K + C_e^n\right)^{1/n}}, \tag{6}$$

where q_m is a constant measured in mg g^{-1}, K is a constant (L^n mg^{-n}), and n is an exponent, which can take values in a wide range (>0), allowing to suitably predict the adsorption isotherms.

The isotherm model of Khan was developed for studying the adsorption of aromatic compounds on activated carbons from multicomponent aqueous phase solutions [43–45]. The generalized model for a single solute could be formulated according to Eq. (7),

$$q_e = \frac{q_m \cdot K \cdot C_e}{(1 + K \cdot C_e)^n}, \tag{7}$$

where q_m and K are constants measured in mg g^{-1} and L mg^{-1}, respectively, and n is the exponent.

The model Vieth-Sladek was first proposed to model adsorption of gases in glassy polymers. Owing to the remarkable resemblance of the studied application with the adsorption on porous solids [92] it has been also used to model the adsorption of model pollutants [47,91]. The model may be expressed by Eq. (8),

$$q_e = \frac{q_m \cdot K \cdot C_e}{1 + K \cdot C_e} + n \cdot C_e, \tag{8}$$

where q_m, K and n are constants measured in mg g^{-1} for q_m and L mg^{-1} for both K and n.

Brouers and Sotolongo proposed a Weibull distribution as a possible empirical isotherm model [8] that has been used to predict pollutants adsorption on carbon-based materials [91]. The Brouers and Sotolongo equation is formulated as Eq.(9),

$$q_e = q_m \cdot \left(1 - \exp\left(-K \cdot C_e^n\right)\right), \tag{9}$$

where q_m and K are constants measured in mg g^{-1} and L^n mg^{-n}, respectively, and n is the exponent.

The Jovanović model consists of two equations developed for the physical adsorption on monolayer and multilayer adsorption. Initially, this model was developed for adsorption in the gas phase [41], but it is largely used in the adsorption of solutes from aqueous media solutions [91,93].

2.2. Kinetic adsorption models

The pseudo-first-order equation describes the adsorption rate based on the monolayer adsorption capacity [33] and it is typically represented by Eq. (10):

$$q_t = q_e \cdot (1 - \exp(-k \cdot t)), \tag{10}$$

where q_t and q_e refer the solute adsorbed (Ni(II)) per mass of adsorbent (mg g^{-1}) at a time of contact t (min) and at the equilibria stage, respectively, and k represents the rate constant of the adsorption process (min^{-1}).

The pseudo-second-order model [58], also found as an hyperbolic model [20], is typically used to describe adsorption processes controlled by chemisorption, involving valence forces through sharing or exchange of electrons between the adsorbent and the adsorbate. Eq. (11) represents this model,

$$q_t = \frac{1}{\frac{1}{(k \cdot q_e^2)} \cdot \frac{1}{t} + \frac{1}{(q_e)}}, \tag{11}$$

where the rate constant k is measured in g mg^{-1} min^{-1}.

Bangham is a pore diffusion model expressed by Eq. (12):

$$q_t = k \cdot t^{1/m}, \tag{12}$$

where the rate constant k is measured in mg g^{-1} $min^{-1/m}$ and m is an exponent.

The Elovich equation is a model based on chemical adsorption [70], typically used in the simplified form obtained by Chien and Clayton [20]. In this work, the integrated form of Elovich equation was used, as shown in Eq. (13),

$$q_t = \frac{1}{\beta} \cdot \ln(\alpha \cdot \beta \cdot t + 1), \tag{13}$$

where α and β (two-parameter model) are the Elovich constants measured in mg g^{-1} min^{-1} and g mg $^{-1}$, respectively.

The Dünwald-Wagner intraparticle diffusion model is typically expressed as shown in Eq. (14) [69],

$$q_t = q_e \cdot \sqrt{1 - \exp(-k \cdot t)}, \tag{14}$$

where the rate constant k is measured in min^{-1} and m is an exponent.

Weber-Morris equation is another mechanistic model typically found as shown in Eq. (15),

$$q_t = k\cdot\sqrt{t} + m, \tag{15}$$

where the rate constant k is measured in mg g^{-1} $min^{-1/2}$ and m is a parameter measured in mg g^{-1}.

The Avrami kinetic model was developed considering possible changes of the adsorption rates as a function of the initial concentration and the adsorption time, as well as the determination of fractionary kinetic orders [56] and it is expressed as in Eq.(16),

$$q_t = q_e\cdot(1-\exp(-k\cdot t)^m), \tag{16}$$

where the rate constant k is measured in min^{-1} and m is an exponent (only three parameter-kinetic adsorption model used in this work).

3. Methodology

3.1. Reagents and materials

Tangerine peels (TP) were obtained after domestic use. 99.995 % nitrogen was supplied from Praxair. 97 % iron (III) chloride hexahydrate ($FeCl_3$.6 H_2O) was supplied from Panreac, 95 % nickel(II) chloride hexahydrate ($NiCl_2$.6 H_2O), 98 % sodium hydroxide (NaOH) and 37 % hydrochloric acid (HCl) were obtained from Fisher chemicals. All reagents were used as received without further purification, and distilled water was used throughout the research.

3.2. Carbon materials preparation

TP was first dried in oven at 100 ºC for 24 h, and then grinded and sieved to obtain particle sizes between 106 and 250 μm using two sieves with metallic mesh (CISA) according to ISO 3310.1 and ASTM E-11–95 (Nº 140 and 60, respectively). Hydrochar microspheres were then produced adapting the methodology described elsewhere [15,16]. Briefly, a suspension of 2.5 g of the dried and sieved TP was prepared with 20 mL of $FeCl_3$ solution (2.5, 1.0 and 0.5 M) in a 125 mL high-pressure autoclave (Model 249 M 4744–49, Parr Instrument co., USA), heated to 200 ºC for 3 h under autogenous pressure. The recovered hydrochar microspheres were labelled as HCMS-2.5, HCMS-1.0, and HCMS-0.5, according to the concentration of $FeCl_3$ solution used in the HTC.

A pyrochar (PC) and activated carbons microspheres (ACMS-2.5, ACMS-1.0, ACMS-0.5 from HCMS-2.5, HCMS-1.0, and HCMS-0.5, respectively) were produced by pyrolysis of the TP and hydrochars, respectively, under N_2 continuous flow (100 Ncm^3 min^{-1}) at 800 ºC, for 4 h, using a tubular furnace (Therm Concept).

3.3. Characterization

The compositions of the solid materials (PC, HCMSs and ACMSs) were determined by elemental analysis (Carlo Erba Instrument EA 1108) to know the weight percentages of carbon, nitrogen, hydrogen and sulfur. To determine ashes, the carbonaceous materials were weighted before and after calcination, conducted in static air (muffle) at 800 ºC for 4 h.

The textural properties of the carbonaceous materials were determined from the analysis of N_2 adsorption-desorption isotherms at 77 K, obtained in a Quantachrome NOVA TOUCH LX4 adsorption analyzer. Degasification was conducted for 16 h at 120 ºC. BET, Langmuir, external and microporous surface areas (S_{BET}, $S_{Langmuir}$, S_{ext} and S_{mic}, respectively), micropore volume (V_{mic}) and total pore volume (V_{Total}), were determined as described elsewhere [63].

Scanning electron microscopy (SEM) images of the TP-based carbonaceous materials were obtained using a FEI Quanta 400FEG ESEM/EDAX Genesis X4Minstrument equipped with an Energy Dispersive Spectrometer (EDS).

Functionalities were studied through X-ray photoelectron spectroscopy (XPS) and Fourier-transform infrared spectroscopy (FT-IR). XPS analysis was conducted in a PHI-5701 of Physical Electronics, whereas FT-IR spectra were obtained with a Perkin Elmer FT-IR spectrophotometer UATR Two with a resolution of 1 cm^{-1} and scan range of 3000–450 cm^{-1}.

Acidity and basicity of the carbon-based materials were determined by acid-base titration of an acid or base solution after keeping in contact with the adsorbents for 48 h, as detailed in the literature [18,73]. Surface acidity (SA) and basicity (SB) were determined considering the BET surface area of each adsorbent.

3.4. Ni(II) adsorption runs

Equilibrium adsorption isotherms of Ni(II) on the ACs, PC and HCs were determined by means of the equilibrium method [19]. First, 0.125 g of adsorbent were added into 50 mL of nickel(II) chloride solutions at different concentrations (5, 10, 20, 50, 80 and 100 mg L^{-1} of Ni(II)). The mixtures were stirred at 240 rpm for 72 h.

Kinetic adsorption of Ni(II) on the TP-based materials was conducted using 0.125 g of adsorbent and 50 mL of a 5 mg L^{-1} nickel(II) chloride solution. The adsorption was conducted at 240 rpm. Then, different samples were withdrawn from the Erlenmeyer at the following selected times: 15, 30, 60, 120, 240 and 1440 min

The effect of pH in the adsorption of Ni(II) onto the TP-based adsorbents was assessed at pH ranging from 3 to 9. For each run, 50 mL of the 100 mg L^{-1} Ni(II) chloride solution was used and 0.125 g of the adsorbent was added. The pH of the solution was adjusted using 1 mol L^{-1} HCl and 1 mol L^{-1} NaOH during all runs. After 72 h, the samples were filtered in order to separate the adsorbent from the liquid fraction and the concentration of Ni (II) in the filtrate was determined.

Samples withdrawn during the adsorption experiments were filtered to separate the adsorbent, and the liquid samples were analyzed by atomic absorption spectrophotometry (Varian SpectrAA 220, Steinhausen, Switzerland) to determine Ni(II) in the aliquots.

3.5. Modelling and calculation methods

The amount of Ni(II) adsorbed on the TP-based materials was determined by application of Eq. (17),

$$q_t = \frac{\left(C_{Ni(II),0} - C_{Ni(II),t}\right)\ V}{W_{adsorbent}}, \tag{17}$$

where q_t refers to the amount of Ni(II) adsorbed per unit mass of TP-based material at time t (mg g^{-1}), $C_{Ni(II),0}$ is the initial Ni(II) concentration in the aqueous solution (mg L^{-1}), $C_{Ni(II),t}$ is the concentration of Ni(II) in the solution at the adsorption time t (mg L^{-1}), $W_{adsorbent}$ refers to the mass (g) of TP-based material and V is the volume of the aqueous solution (L).

Kinetic and isotherm adsorption models were obtained using non-linear regression since better-fitted equations are obtained than using linearized equations [49], consisting of successive numerical iterations to minimize the least sum of squared errors (SSE) of q_t (*cf.* Eq. (18)), as detailed in previous works dealing with modeling methods [17,20],

$$SSE = \sum_{i=1}^{n}\left(q_{t,exp,i} - q_{t,model,i}\right)^2, \tag{18}$$

where $q_{t,exp,i}$ (mg g^{-1}) is the amount of Ni(II) adsorbed per unit mass of TP-based adsorbent at time t in the measured adsorption experiments (q_t being expressed as q_e for equilibrium runs), $q_{t,model,i}$ (mg g^{-1}) the respective calculated values given by the model, i representing each value up to n values obtained in each experiment.

Table 1
Elemental composition of the carbonaceous materials based on tangerine peels.

Sample	C/H	C (wt%)	H (wt%)	N (wt%)	S (wt %)	Ash (wt %)	Remaining content[a] (wt %)
TP	6.8	42.1 ± 0.1	6.17 ± 0.03	0.77 ± 0.05	0.05 ± 0.03	4.4 ± 1.4	46.5
HCMS-0.5	12.4	64.7 ± 0.3	5.21 ± 0.09	0.69 ± 0.09	0.05 ± 0.01	1.4 ± 0.2	28.0
HCMS-1.0	12.9	65.0 ± 0.2	5.02 ± 0.06	0.60 ± 0.04	0.03 ± 0.01	3.2 ± 1.6	26.1
HCMS-2.5	13.9	65.9 ± 0.2	4.74 ± 0.05	0.44 ± 0.02	0.03 ± 0.01	4.8 ± 2.1	24.0
PC	57.2	79.4 ± 0.4	1.39 ± 0.02	1.63 ± 0.01	0.03 ± 0.01	8.0 ± 0.4	9.6
ACMS-0.5	77.0	93.1 ± 0.2	1.21 ± 0.04	1.01 ± 0.05	0.03 ± 0.02	2.2 ± 0.3	2.5
ACMS-1.0	75.8	90.8 ± 1.0	1.20 ± 0.00	0.86 ± 0.02	0.04 ± 0.01	3.3 ± 1.0	3.8
ACMS-2.5	82.8	87.6 ± 1.5	1.06 ± 0.03	0.02 ± 0.01	0.03 ± 0.03	5.1 ± 0.6	6.2

[a] Obtained by the difference: 100 %-C(%)-H(%)-N(%)-S(%)-Ash(%).

Alternatively, different error functions were used, *viz.* the sum of the square of the errors (*SSE*), the sum of absolute errors (*SAE*), the hybrid error function (*HYBRYD*), the Marquard's percent standard deviation (*MPSD*), and the average relative error (*ARE*) [42] to assure the good fitness of the models. *SAE*, *HYBRYD*, *MPSD*, and *ARE* error functions are respectively described by Eqs. (19–22),

$$SAE = \sum_{i=1}^{n} \left| q_{t,exp,i} - q_{t,model,i} \right|, \tag{19}$$

$$HYBRYD = \frac{100}{n-p} \sum_{i=1}^{n} \frac{\left(q_{t,exp,i} - q_{t,model,i} \right)^2}{q_{t,exp,i}}, \tag{20}$$

$$MPSD = 100 \sqrt{\frac{1}{n-p} \sum_{i=1}^{n} \left(\frac{q_{t,exp,i} - q_{t,model,i}}{q_{t,exp,i}} \right)^2}, \tag{21}$$

$$ARE = \frac{100}{p} \sum_{i=1}^{n} \left| \frac{q_{t,exp,i} - q_{t,model,i}}{q_{t,exp,i}} \right|, \tag{22}$$

where p refers to the number of parameters for each model (remaining parameters as above described for *SSE*).

The models were also evaluated by the determination factor (r^2) and the adjusted determination factor ($r^2_{adjust.}$), to take into account the degrees of freedom or the number of parameters from each model equation [28].

4. Results and discussion

4.1. Composition of TP-based adsorbents

Table 1 summarizes the carbon, hydrogen, nitrogen, sulfur and ash contents for the precursor (TP) and for the prepared carbonaceous materials. Compared to the raw waste (42.1 wt % and 6.17 wt% of C and H, respectively), it is possible to observe that the carbon content increases (64.7–93.1 wt%) and the hydrogen composition decreases (1.06–5.21 wt%) for all TP-based materials prepared, resulting in an increment of the C/H ratio (from 6.8 in the TP precursor to 12.4–82.8 in the prepared materials). The effect is more evident in materials subjected to pyrolysis (ACMSs and PC) since the thermal process causes the release of volatile compounds, such as water and low molecular weight hydrocarbons, and the carbonization of the sample [12,16].

The increase in the C/H ratio observed for hydrochars (12.4–13.9) with respect to TP (6.82) is due to aromatization, condensation or polycyclization reactions during the carbonization of TP [12,16]. ACs (ACMS-2.5, ACMS-1.5 and ACMS-0.5) prepared by sequential HTC and pyrolysis show the highest C/H ratios (77.0–82.8), due to the effect of both processes. Among the ACMSs and HCMSs, ACMS-2.5 and HCMS-2.5 show the highest C/H ratios (82.8 and 13.9), evidencing the role played by the iron catalyst during the carbonization processes.

The ash content in the TP and in the carbon-based materials is a measure of the inert, inorganic and probably unusable part of the material whose presence may modify the interaction between the surface of the carbon material and the adsorbate [6]. The TP-based materials show values of ashes ranging from 1.4 to 8.0 wt%. The highest value was found for PC since pyrolysis leads to the volatilization of the organic compounds of the precursor TP, as also observed in works dealing with the production of carbon materials from other sources [16]. The same effect was observed for ACMSs (2.2–5.1 wt% of ashes) prepared by pyrolysis from HCMS (1.4–4.8 wt% of ashes). On the other hand, HTC leads to a decrease in the ash content, likely due to the leaching of alkali and alkaline earth metals present in the TP, promoted by the contact of the solid with the high temperature liquid solution, as was observed in previous works dealing with HTC or using acid solutions during the activation of ACs [16,17,71]. Only one hydrochar (HCMS-2.5) shows a slight increase of ash content (from 4.4 to 4.8 wt%), which was ascribed to the impregnation of the material with iron during HTC, as evidenced by the tendency of increasing ash content with increasing iron concentration: 4.8, 3.2 and 1.4 wt% for hydrochars prepared with 2.5, 1.0 and 0.5 M of $FeCl_3$, respectively.

The remaining content (different from C, H, N, S and ashes) is typically associated with other heteroatoms, such as oxygen. As observed, its content decreases after either pyrolysis or HTC due to the carbonization processes (those elements are released).

4.2. Porosity and Ni(II) uptake capacity

The N_2 adsorption isotherms of the studied TP-based adsorbents are depicted in Fig. S1 and the textural properties obtained through the calculation methods described in the methodology are summarized in

Table 2
Textural properties of the carbonaceous materials prepared from tangerine peels.

Sample	S_{BET} ($m^2\ g^{-1}$)	$S_{Langmuir}$ ($m^2\ g^{-1}$)	S_{ext} ($m^2\ g^{-1}$)	S_{mic} ($m^2\ g^{-1}$)	V_{mic} ($mm^3\ g^{-1}$)	V_{Total} ($mm^3\ g^{-1}$)	q_e[a] (mg g^{-1})	Q_e[a,b] (μg m^{-2})
HCMS-0.5	7	6	7	0	0	15	0.19	27.8
HCMS-1.0	7	6	7	0	0	17	0.38	54.8
HCMS-2.5	11	11	11	0	0	27	0.60	54.6
PC	104	146	10	94	50	66	1.99	19.1
ACMS-0.5	238	330	34	204	108	162	0.40	1.7
ACMS-1.0	262	349	64	198	101	213	0.79	3.0
ACMS-2.5	287	391	70	217	116	282	1.43	5.0

[a] Uptake capacities of Ni for each adsorbent were obtained using $C_{Ni(II),0}$ of 5 mg L^{-1} and 2.5 g L^{-1} of adsorbent.
[b] Q_e was determined as q_e/S_{BET}.

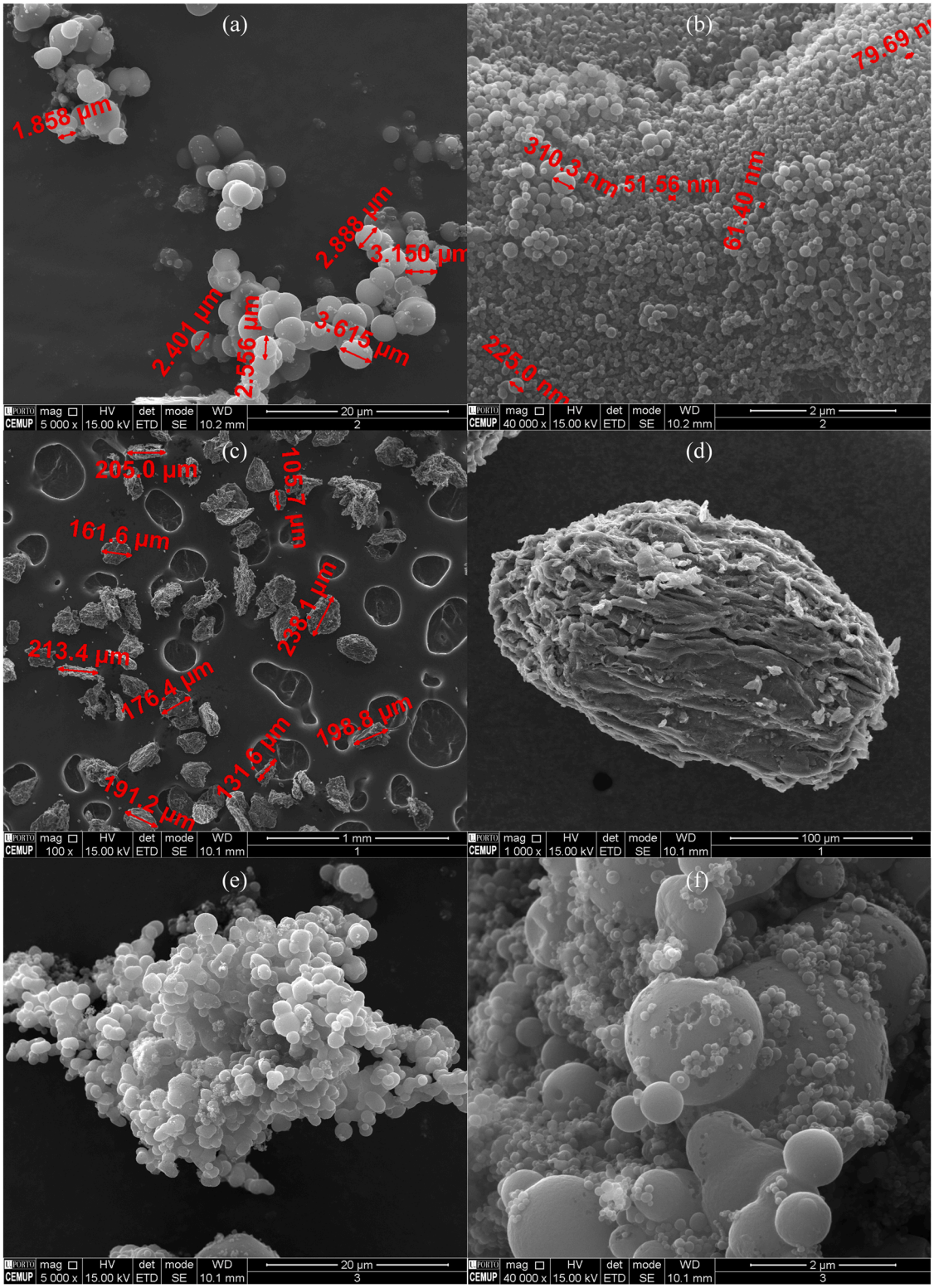

Fig. 1. SEM micrographs of carbonaceous adsorbents obtained from TP: (a-b) HCMS-2.5, (c-d) PC and (e-f) ACMS-2.5.

Table 2. As observed, nitrogen adsorption isotherms show higher quantities of volume adsorbed for ACMSs, followed by PC and HCMSs, whose uptake capacity is considerably lower. Similar trend has been reported in studies dealing with the preparation of ACs, PCs and HCs and from different precursors [16].

As expected, ACMSs have the highest BET (238–287 $m^2\ g^{-1}$) and Langmuir (330–391 $m^2\ g^{-1}$) surface areas and total pore volumes (162–282 $mm^3\ g^{-1}$), among all adsorbents prepared. ACMSs show similar results to those reported in the literature regarding the synthesis of carbon materials prepared by diverse activation and carbonization methods of rice husk (171–280 $m^2\ g^{-1}$) [13,64], palm shell (260–266 $m^2\ g^{-1}$) [14,31], or coconut shell (183 $m^2\ g^{-1}$) [14].

The PC sample, obtained by pyrolysis of TP without any other treatment, reaches values considerably lower than ACMSs (104 and

146 $m^2\ g^{-1}$ of BET and Langmuir specific surface areas, respectively and 66 $mm^3\ g^{-1}$ of total pore volume), evidencing that HTC works as activation process for the development of ACMSs. The PC sample presents a significant microporosity (S_{mic} = 94 $m^2\ g^{-1}$ and V_{mic} = 50 $mm^3\ g^{-1}$), showing that citric peels are interesting precursors for the development of carbon-based adsorbents. Obviously, microporosity increases when HTC is used prior to pyrolysis, obtaining ACs instead of PC, resulting in materials with a microposity two times higher than that in PC (S_{mic} = 198–217 $m^2\ g^{-1}$ and V_{mic} = 101–116 $mm^3\ g^{-1}$).

Moreover, the differences found among the ACMSs evidence the effect of the quantity of iron impregnating the HCs as an active catalyst for the carbonization and development of porosity, since specific surface areas and total pore volume increase in the following order ACMS-0.5 <ACMS-1.0 <ACMS-2.5. Similar values are found in the literature [16,71] for the specific surface areas and pore volume of HCs that were determined according to the nitrogen adsorption isotherms (Fig. S1).

Preliminary tests related to the adsorption of Ni(II) (in 5 mg L^{-1} aqueous solution) over the TP-based carbonaceous materials (2.5 g L^{-1} of adsorbent) at room temperature reveal that is possible to remove an amount of the heavy metal from the aqueous solution per unit mass of the adsorbent ranging from 0.19 to 1.99 mg per g of adsorbent (*cf.* Table 2), being the highest uptake capacity of Ni(II) obtained with the PC adsorbent, *i.e.,* the pyrochar. Although ACs show more interesting textural properties for this application (highest specific surface areas and total pore volumes); however, lower adsorption capacities are obtained with ACMSs (1.43–0.40 mg g^{-1}) when compared to the pyrochar (1.99 mg g^{-1}). On the other hand, HCMSs show some unexpected uptake capacity (0.60–0.19 mg g^{-1}), when considering their textural properties. In fact, the capacity of adsorption per surface area (Q_e) of these materials is significantly higher (27.8–54.8 μg m^{-2}) than that of PC (19.1 μg m^{-2}) and ACMSs (1.7–5.0 μg m^{-2}).

It is noteworthy that the largest uptake capacities among ACMSs (1.43 mg g^{-1}) and HCMSs (0.60 mg g^{-1}) were obtained for the TP-based adsorbents prepared with the highest concentration of $FeCl_3$ during the HTC (ACMS-2.5 and HCMS-2.5). For this reason, only these materials were selected for further investigation.

4.3. Morphology

Texture and morphology of three selected TP-based adsorbents (HCMS-2.5, PC and ACMS-2.5) were determined through SEM (*cf.* Fig. 1). The microphotographs confirm the production of microspheres by HTC using $FeCl_3$. For HCMS-2.5, it is possible to observe particle sizes ranging from 1858 to 3615 nm at low image magnification (Fig. 1a), but many carbon microspheres were found with sizes between 50 and 350 nm (Fig. 1b).

The material prepared by pyrolysis of TP without further physical-chemical treatment (PC) presents higher particle sizes (105.7–238.1 μm) than HCMS-2.5 and ACMS-2.5 (Fig. 1c). The particle size of PC is in accordance with the sieving performed to prepare the adsorbents (sieves with a metallic mesh to separate particle sizes between 106 and 250 μm). The implication is that the particle size of the precursor is not strongly affected by pyrolysis, as it is by HTC with $FeCl_3$, which led to decrease more than 100 times the particle size. Regarding the morphology, PC shows irregular particle shape and a rough surface, likely due to the porosity developed during the pyrolysis to prepare PC.

The pyrolysis of HCMS-2.5 to obtain ACMS-2.5 allowed to keep the particle size of microspheres, although it is possible to observe the sintering of some microspheres of HCMS-2.5, leading to agglomeration of activated carbon microspheres (Fig. 1e). The surface of this material is also slightly rough, probably due to the porosity development during the thermal treatment, as observed for PC.

Selected regions of micrographs were analysed by EDS to determine the elemental content of HCMS-2.5, PC and ACMS-2.5 (Fig. S2). As observed, the materials mainly consist of carbon. HCMS-2.5 (Fig. S2a) and ACMS-2.5 (Fig. S2c) show a slight iron content. On the other hand, the EDS of PC adsorbent confirms the presence of alkali and alkaline earth metals (Na, Mg, K and Ca) from the precursor. The presence of this metal and the highest signal in oxygen for PC compared to ACMS-2.5 is in accordance with the CHNS-elemental analysis presented above. Alkali and alkaline earth metals were not detected for HCMS-2.5, nor ACMS-2.5, meaning that HTC allows to obtain more purified carbonized adsorbents.

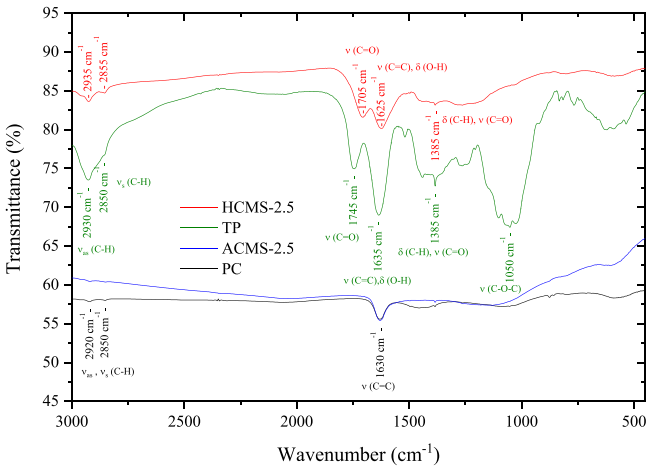

Fig. 2. FT-IR spectra of raw TP and selected adsorbents (HCMS-2.5, PC and ACMS-2.5).

4.4. Surface chemistry

The adsorptive properties of carbonaceous adsorbents are influenced not only by their textural properties but also by their surface chemistry. TP-based adsorbents may contain heteroatoms such as oxygen, nitrogen and phosphorus on their surface that form organic functional groups, such as carbonyls, carboxylic acids, lactones, ethers, phenols, aldehydes, amines and phosphates, which can be neutral, acidic or basic [40]. The surface chemistry depends on the composition of the precursor and on the method of carbonization [7,30]. Fig. 2 shows FT-IR spectra obtained for the TP precursor and the selected adsorbents (ACMS-2.5, PC and HCMS-2.5). The bands were assigned to probable bounds according to FT-IR spectra of diverse carbon-based materials [90].

As observed, the TP precursor presents more bands than the respective TP-based carbon materials due to the complex composition of the biomass. As a C-rich material, some bands can be ascribed to the presence of C-H (2930–2850 cm^{-1}) and C═C (1635 cm^{-1}) bonds.

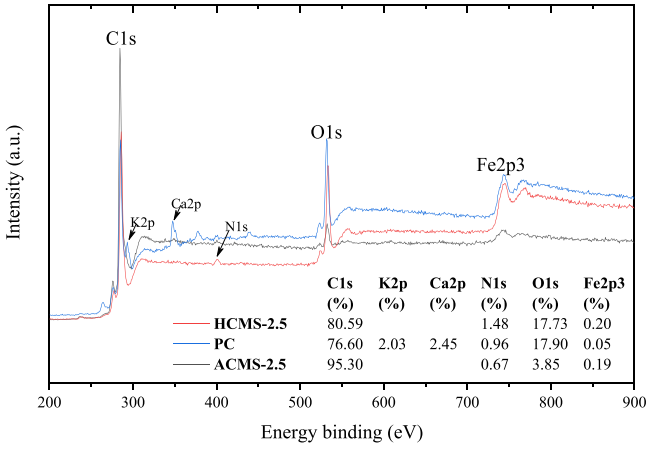

	C1s (%)	K2p (%)	Ca2p (%)	N1s (%)	O1s (%)	Fe2p3 (%)
HCMS-2.5	80.59			1.48	17.73	0.20
PC	76.60	2.03	2.45	0.96	17.90	0.05
ACMS-2.5	95.30			0.67	3.85	0.19

Fig. 3. XPS spectra and atomic percentage of elements on the surface of TP-based adsorbents.

Table 3
Binding energy assignment for oxygen functional groups and their atomic percentage content on the adsorbents' surface.

Binding energy (eV)	Functional group	HCMS-2.5 (%)	ACMS-2.5 (%)
531.1	Carbonyl (C═O)	2.1	1.5
532.3	Hydroxyls groups (-O-H)	14.7	0.7
533.3	C–O in esters and anhydrides	0.8	0.9
534.2	Carboxylic groups	0.1	0.4
536.1	Water	0.1	0.3
	TOTAL	17.7	3.9

Table 4
Acid-based properties of the carbonaceous materials based on tangerine peels.

Sample	Acidity (mmol g^{-1})	SA[a] (μmol m^{-2})	Basicity (mmol g^{-1})	SB[a] (μmol m^{-2})
HCMS-2.5	0.32	45.7	0.21	30.4
PC	0.01	0.10	1.83	17.6
ACMS-2.5	0.23	0.78	0.70	2.44

[a] Surface acidity (SA) and basicity (SB) was determined as acidity/S_{BET} and basicity/S_{BET}, respectively.

However, this material stands out for the high content of surface oxygen groups (SOGs). Hydroxyl groups (-O-H) are found at 1635–1625 cm^{-1}. Carbonyls (-C═O) can be identified at 1385 cm^{-1} and the presence of epoxy groups are demonstrated by bands at 1050, 1075 and 1150 cm^{-1}. The carbonized samples (HCMS-2.5, PC and ACMS-2.5) show a strong decrease in the bands representative of SOGs. In fact, PC and ACMS-2.5 only present a significant band at 1630 cm^{-1} that can be assigned to double bounds between carbon atoms. The absence of significant bands for C—H bonds and SOGs demonstrated the success of the carbonization and a poor functionalized surface. The lower content of O and H agrees with the elemental composition found by elemental analysis. On the other hand, HCMS-2.5 show significant bands at 2930–2850 cm^{-1} (C—H bonds) and the regions of diverse SOGs, as expected for the hydrothermal treatment at low temperatures, also agreeing with the results for elemental analysis.

Fig. 3 shows the XPS spectra and the relative atomic percentage content of elements on the surface of each TP-based adsorbent. As expected, HCMS-2.5 corresponds to hydrochar microspheres rich in surface oxygen groups (SOGs), since 17.73 % of O1s was obtained. Surprisingly, PC also presents a high content of oxygen on the surface and this technique also confirms the presence of metals (K and Ca). The values obtained are close to those obtained by SEM/EDS and also similar to the elemental composition obtained by CHNS-AE. K and Ca were not detected in ACMS-2.5 and HCMS-2.5, as HTC can remove those elements, as corroborated by SEM/EDS. ACMS-2.5 shows the lowest content of oxygen and the highest content of C among the selected materials, agreeing with the results obtained by elemental analysis. As observed, most of iron was removed from the microsphere materials (HCMS-2.5 and ACMS-2.5) after washing. On the other hand, the low iron content observed for PC most likely comes from the raw TP used as a precursor.

To deepen knowledge of the surface chemistry, O1s peaks of XPS spectra analysis were assessed for the materials without significant quantities of other metals, *i.e.*, HCMS-2.5 and ACMS-2.5. O1s deconvolution curves are represented in Fig. S3 and the assignments to the relative content of SOGs are summarized in Table 3. As observed, HCMS-2.5 presents mainly hydroxyl groups (14.7 % out of 17.7 %), whereas ACMS-2.5 shows lower content of hydroxyl groups with a more predominant presence of carbonyl groups (1.5 % out of 3.9 %). The reduction of hydroxylic groups in ACMS-2.5 can be ascribed to the release of weak hydroxyl groups during the pyrolysis at 800 °C of HCMS-2.5 to obtain ACMS-2.5.

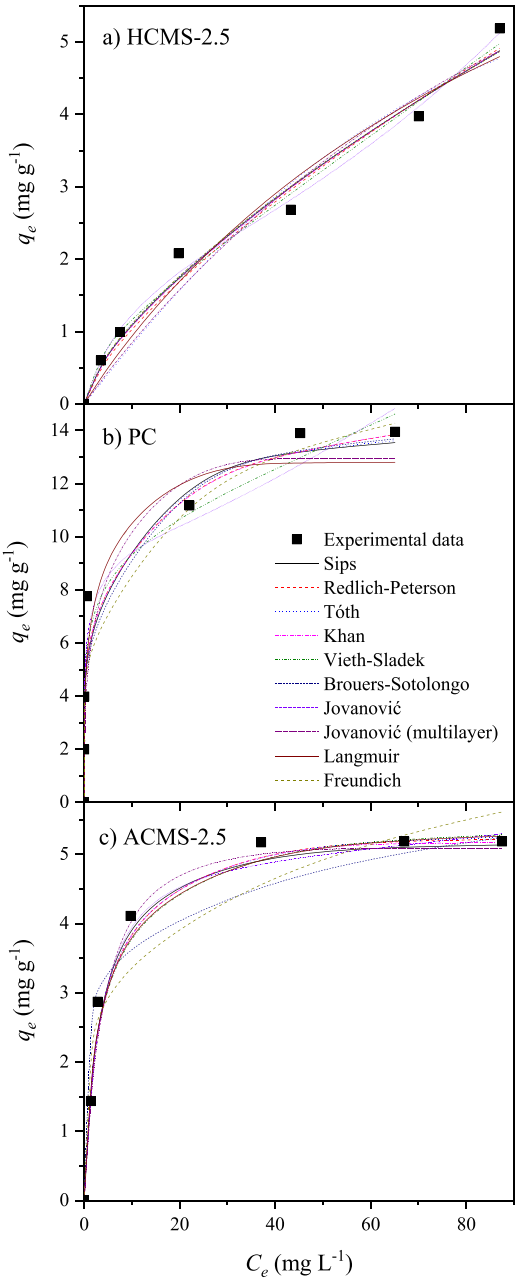

Fig. 4. Isotherm adsorption of Ni(II) on (a) HCMS-2.5, (b) PC and (c) ACMS-2.5 TP-based adsorbents and fitted isotherm adsorption models (Operating conditions: C_{ads} = 2.5 g L^{-1}, room temperature, and $C_{Ni(II),0}$ = 5–100 mg L^{-1}).

The results obtained in terms of acidity and basicity of the selected adsorbents (ACMS-2.5, PC and HCMS-2.5) are shown in Table 4. As can be seen, acid-base properties show significant differences among the adsorbents, hydrochar HCMS-2.5 being more acid (0.32 mmol g^{-1}) than ACMS-2.5 (0.23 mmol g^{-1}) and, especially, than PC (0.01 mmol g^{-1}). Taking into account the specific surface area of the materials, the same order is observed for the surface acidity: HCMS-2.5 (45.7 μmol m^{-2}) > ACMS-2.5 (0.78 μmol m^{-2}) > PC (0.10 μmol m^{-2}). On the opposite, the basic character of the adsorbents follows a different order when measured per mass or per surface area, highlighting the basicity of PC (1.83 mmol g^{-1}) and HCMS-2.5 (30.4 μmol m^{-2}). Interestingly, the same order was found for the basicity (Table 4) and the uptake capacity of the materials (Table 2) per gram (PC > ACMS-2.5 > HCMS-2.5) and per

Table 5
Parameter values and statistical data obtained from the fitting of the isotherm models to the adsorption runs with HCMS-2.5, PC, and ACMS-2.5 (units: mg for pollutant, g for adsorbent, L for volume).

Model	Non-linear form	Sample	q_m	K	n	SSE	r^2	$r^2_{adjust.}$
Sips	$q_e = \frac{q_m \cdot K \cdot C_e{}^n}{1 + K \cdot C_e{}^n}$	HCMS-2.5	2323	$1{\cdot}10^{-4}$	0.682	0.37	0.976	0.961
		PC	15.7	1.07	0.430	3.59	0.972	0.954
		ACMS-2.5	5.20	0.287	1.26	0.15	0.989	0.981
Redlich-Peterson	$q_e = \frac{A \cdot C_e}{1 + K \cdot C_e^n}$	HCMS-2.5	0.209	64.7	0.292	0.39	0.977	0.962
		PC	8.51	21.6	0.883	1.91	0.985	0.975
	$(q_m = A/K)$	ACMS-2.5	6.16	0.266	1.029	0.15	0.988	0.980
Tóth	$q_e = \frac{q_m \cdot C_e}{\left(1/K + C_e^n\right)^{1/n}}$	HCMS-2.5	6.16	$1{\cdot}10^{-4}$	2.131	0.97	0.955	0.925
		PC	17.7	4.07	0.279	3.14	0.976	0.959
		ACMS-2.5	5.36	0.254	1.131	0.15	0.988	0.981
Khan	$q_e = \frac{q_m \cdot K \cdot C_e}{(1 + K \cdot C_e)^n}$	HCMS-2.5	0.00	379.8	0.314	0.37	0.977	0.961
		PC	5.62	27.7	0.880	1.80	0.986	0.977
		ACMS-2.5	6.37	0.253	1.05	0.16	0.987	0.979
Vieth-Sladek	$q_e = \frac{q_m \cdot K \cdot C_e}{1 + K \cdot C_e} + n \cdot C_e$	HCMS-2.5	0.97	0.308	0.046	0.25	0.984	0.973
		PC	9.26	12.8	0.082	1.80	0.986	0.977
		ACMS-2.5	5.45	0.324	$1{\cdot}10^{-4}$	0.17	0.986	0.977
Brouers-Sotolongo	$q_e = q_m \cdot \left(1 - \exp\left(-K \cdot C_e^n\right)\right)$	HCMS-2.5	169.9	$1.4{\cdot}10^{-3}$	0.680	0.38	0.976	0.960
		PC	14.96	0.701	0.301	4.22	0.968	0.946
		ACMS-2.5	244.4	0.011	0.156	2.34	0.885	0.809
Jovanović (multilayer)	$q_e = q_m \cdot (1 - \exp(-K \cdot C_e)) \cdot \exp(n \cdot C_e)$	HCMS-2.5	1.53	0.137	0.014	0.07	0.996	0.993
		PC	8.81	11.6	$8.0{\cdot}10^{-3}$	4.03	0.969	0.948
		ACMS-2.5	4.63	0.295	$1.5{\cdot}10^{-3}$	0.27	0.977	0.962
Jovanović (monolayer)	$q_e = q_m \cdot (1 - \exp(-K \cdot C_e))$	HCMS-2.5	7.40	0.012		0.76	0.966	0.958
		PC	12.9	1.77		16.18	0.934	0.918
		ACMS-2.5	5.08	0.243		0.39	0.968	0.961
Langmuir	$q_e = \frac{q_m \cdot K \cdot C_e}{1 + K \cdot C_e}$	HCMS-2.5	9.96	0.011		0.69	0.962	0.953
		PC	12.9	4.26		10.94	0.930	0.912
		ACMS-2.5	5.44	0.334		0.18	0.987	0.983
Freundlich	$q_e = K \cdot C_e^{1/n}$	HCMS-2.5		0.24	0.671	0.37	0.976	0.970
		PC		6.76	0.179	5.44	0.958	0.948
		ACMS-2.5		2.14	0.215	1.63	0.866	0.833

surface area (HCMS-2.5 > PC > ACMS-2.5), evidencing the strong role played by the basicity in the adsorption of Ni(II).

The highest acidity of HCMS-2.5 can be ascribed to the chloride precursor ($FeCl_3$) used as activating agent during HTC. The strong acid and basic character of this material compared to the others are due to the carbonization in the presence of water that leads to a material highly functionalized with oxygen-containing surface groups [4]. This can be expected by the oxygen content of hydrochars according to the remaining content presented in Table 1 (24.0–28.0 wt% for HCMSs, whereas 2.5–9.6 wt% was found for PC and ACMSs). The basicity of PC may be ascribed to the fact of having the highest content of ashes (8.0 wt %, whereas less than 5.1 wt% is found for other TP-based adsorbents), consisting mainly of alkali and alkaline earth metals, as observed both in SEM/EDS and XPS analysis.

4.5. Equilibrium adsorption of Ni(II)

Fig. 4 shows the isotherm adsorption of Ni(II) on the selected adsorbents: (a) HCMS-2.5, (b) PC and (c) ACMS-2.5. As observed, PC shows the highest uptake capacity of Ni(II), reaching values of 13.9 mg g^{-1} at the highest tested initial concentration of Ni(II) ($C_{Ni(II),0} = 100$ mg L^{-1}). In contrast, the highest adsorption capacity of ACMS-2.5 and HCMS-2.5 was 5.18 and 4.88 mg g^{-1}, respectively, at the same operating conditions.

The shape of the isotherms is also considerably different among the TP-based adsorbents. Giles classification is usually used to distinguish the isotherm adsorption curves according to their characteristic shapes between four isotherm classes: high affinity (H), Langmuir (L), constant partition (C) and sigmoidal-shaped (S) [29]. H and L isotherms have a convex shape. However, the slopes of H isotherms reach higher values than L isotherms because the sorption affinity of H isotherms strongly increases with decreasing concentration. S isotherms have a concave shape at low concentrations, while C isotherms are defined by a constant sorption affinity [34].

Accordingly, the isotherm curve obtained with ACMS-2.5 may be classified as L1 since it describes a medium affinity at low concentrations of Ni(II) and equilibrium uptake capacities (q_e) gradually describe an asymptotic curve for C_e higher than approximately 20 mg L^{-1}. The isotherm curve obtained with PC may be classified as H1, since it describes a similar curve, but it shows a strong affinity at a low concentration of Ni(II). The isotherm curve obtained with HCMS-2.5 may be classified as C1, because of the line trend described by the equilibrium uptake capacities upon the initial concentration of Ni(II). These differences may be ascribed to the different textural and acid-base properties of the adsorbents. PC should present the highest affinity and uptake capacity for the combination of a significant porosity and basicity, whereas HCMS-2.5 has not enough specific surface area and ACMS-2.5 shows limited functionality.

The isotherms for adsorption of Ni(II) onto the TP-based adsorbents were evaluated by 10 models: 7 with three parameters (Sips, Redlich-Peterson, Tóth, Khan, Vieth-Sladek, Brouers-Sotolongo and Jovanović for multilayer adsorption), and 3 with two parameters (Jovanović for monolayer adsorption, Langmuir and Freundlich) in their functions [20]. Those models were fitted by a non-linear regression method, since model parameters may be distorted by linear regressions [49,54] and adjusted determination factor ($r^2_{adjust.}$) used to take into account the number of parameters from each model function [20]. The equations, the parameter values and the most significant statistical data obtained from the fitting of the isotherm adsorption models to the experimental data are compiled in Table 5 (isotherm curves obtained are depicted in Fig. 4). As observed, most of the isotherm models accurately fit (r^2 = 0866 – 0.996 and $r^2_{adjust.}$ = 0.809 – 0.993) to the experimental data obtained with the TP-based adsorbents. The fitting with all models considered the minimization of different error functions (*SSE*, *SAE*, *HYBRYD*, *MPSD* and *ARE*), since other studies reported about the importance of the objective function in the fitting with the models [42, 48]). However, non-significant differences were observed among the models for the parameter and statistical data (r^2), as exemplified by the q_m values predicted using *SSE*, *SAE*, *HYBRYD*, *MPSD*, and *ARE* for each isotherm model in Fig. S4. For this case, the maximum difference for the

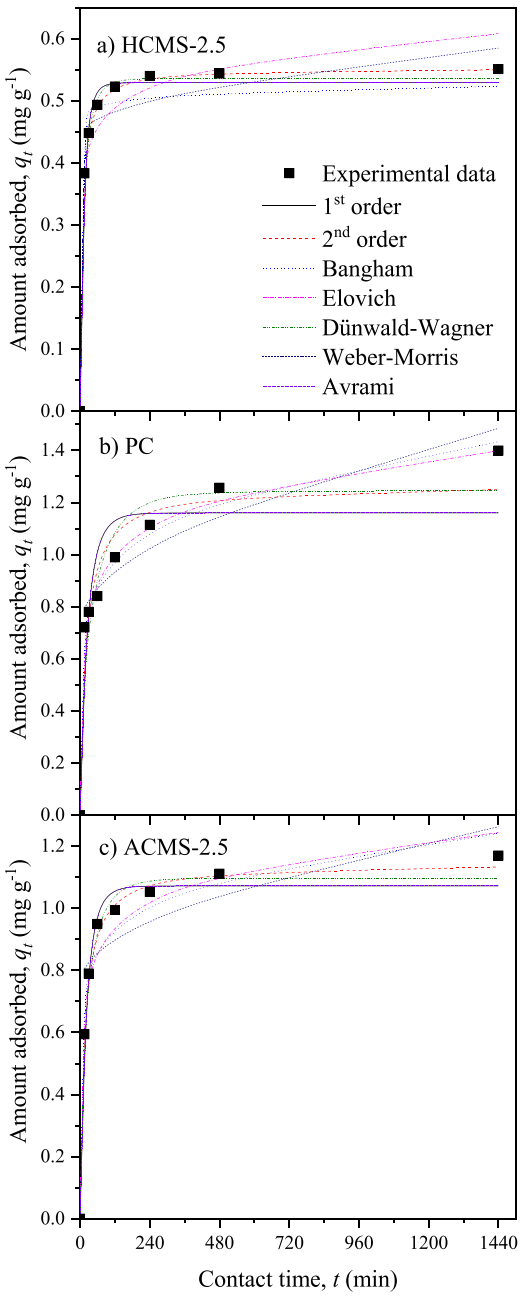

Fig. 5. Kinetic adsorption of Ni(II) on (a) HCMS-2.5, (b) PC and (c) ACMS-2.5 (Operating conditions: C_{ads} = 2.5 g L^{-1}, room temperature, and $C_{Ni\ (II),o}$ = 5 mg L^{-1}).

predicted value of q_m was 2.8 mg g^{-1} found for the Tóth model (simplified function). It is noteworthy that the isotherm models keep the same order of values for the predicted q_m regardless of the error functions used for the fitting, as follows: Tóth > Sips > Brouers-Sotolongo > Langmuir > Jovanović (monolayer) > Vieth-Sladek > Redlich-Peterson > Jovanović (multilayer) > Khan > Freundlich. A similar trend was observed in a previous work [20], so it may be expected to predict higher values of monocape uptake capacity (q_m) with the models of Tóth (simplified model), Sips, Brouers-Sotolongo, Langmuir and Jovanović (model for monolayer adsorption). Among the TP-based materials tested, PC leads to the highest values of both K and q_m, evidencing it as the material with the highest affinity and uptake capacity.

The isotherm adsorption of Ni(II) on ACMS-2.5 is best represented (r^2 = 0986 – 0.989, and $r^2_{adjust.}$ = 0.977 – 0.983) by hyperbolic isotherm adsorption models (Sips, Redlich-Peterson, Tóth, Khan, Vieth-Sladek and Langmuir), which is in agreement with the sorted L1 type isotherm curve according to Giles classification. Taking into account the degrees of freedom in the fitting ($r^2_{adjust.}$), Langmuir is the best model representing the curve of ACMS-2.5 with q_m = 5.44 mg g^{-1}, K = 0.334 L mg^{-1}, $r^2_{adjust.}$ = 0.983, as also evidenced by the value taken by parameter n (close to 1 as the exponent, and close to 0 for Vieth-Sladek) in the other models. The values of the q_m and K for the Langmuir model obtained through the minimization of the different error functions (*SSE*, *SAE*, *HYBRYD*, *MPSD*, and *ARE*) were similar (5.44–5.50 mg g^{-1}, and 0.289–0.334 L mg^{-1} for q_m and K, respectively).

The adimensional Langmuir separation factors (R_L) predicted from the Langmuir model for each TP-based adsorbent are depicted in Fig. S5. As can be seen, the values of R_L obtained for ACMS-2.5, PC, and HCMS-2.5 range from 0 to 1. Hence adsorption is favorable in all cases, but R_L values show great differences among the TP-based adsorbents. HCMS-2.5 leads to values close to 1, characteristic of linear type isotherms, as is described by this adsorbent (Fig. S1). On the opposite, the adsorbent presenting the highest adsorption capacity (PC) shows values of R_L close to 0, expected for irreversible adsorption.

The isotherm adsorption of Ni(II) obtained with PC is also well described using hyperbolic models (r^2 = 0.930 – 0.986, and $r^2_{adjust.}$ = 0.912 – 0.977) being best represented by Khan (q_m = 5.62 mg g^{-1}, K = 27.7 L mg^{-1}, n = 0.880, $r^2_{adjust.}$ = 0.977) and Vieth-Sladek models (q_m = 9.26 mg g^{-1}, K = 12.8 L mg^{-1}, n = 0.082 L g^{-1}, $r^2_{adjust.}$ = 0.977). The differences obtained by fitting with different error functions were also negligible.

For the isotherm adsorption curve of Ni(II) on HCMS-2.5, the model developed for Jovanović for multilayer adsorption (q_m = 1.53 mg g^{-1}, K = 0.137 L mg^{-1}, n = 0.014 L mg^{-1}) considerably fitted better (r^2 = 0.996 and $r^2_{adjust.}$ = 0.993) than all other models evaluated. In a previous work, Jovanović multilayer isotherm was found to satisfactorily predict the adsorption of a pollutant onto activated carbonaceous materials [20] with the same magnitude for both K and m constant values.

Considering the BET surface area of each TP-based adsorbent, the uptake capacity on the monolayer of HCMS-2.5 could be considered the highest ($Q_m = q_m / S_{BET}$ = 139 μg m^{-2}). In this case, the values of the parameters obtained using different error functions were also similar.

4.6. Adsorption kinetics of Ni(II)

The adsorption of Ni(II) from aqueous solution ($C_{Ni(II),0}$ = 5 mg L^{-1}) upon time of contact with 2.5 g L^{-1} of ACMS-2.5, PC, and HCMS-2.5 is represented in Fig. 5. Although HCMS-2.5 shows the lowest adsorption capacity, the adsorption of Ni(II) on HCMS-2.5 is faster compared to ACMS-2.5 and PC, likely due to the absence of microporosity. In contrast, internal diffusion may be hindered in PC and ACMS-2.5. As a consequence, kinetic adsorption on HCMS-2.5 shows an asymptotic trend that is quickly reached, and the equilibrium uptake capacity should be achieved fast.

The assessment of the kinetic adsorption of Ni(II) on the TP-based adsorbents was evaluated using pseudo-first-order, pseudo-second-order, Bangham, Elovich, Dünwald-Wagner, Weber-Morris, and Avrami kinetic models. The equation of these models, the kinetic constants and the statistical data resulting from their fitting to the experimental data obtained in the adsorption of Ni(II) on ACMS-2.5, PC, and HCMS-2.5 are summarized in Table 6. Those models were also fitted by a non-linear regression method [49,54] ($r^2_{adjust.}$ was not presented, since only one model has three parameters – Avrami – and it is not the model best able to predict the data obtained).

The kinetic adsorption curves on the TP-based adsorbents predicted by the models are represented in Fig. 5. As observed, most of the kinetic models are capable of accurately predicting the experimental data obtained and, except for the Weber-Morris for ACMS-2.5 and HCMS-2.5 (r^2 = 0.532–0.647), well fitness is available for the kinetic models to predict the kinetic adsorption curves of the TP-based adsorbents (r^2 =

Table 6
Kinetic parameter values and statistical data obtained from the models fitting to the adsorption runs with HCMS-2.5, PC, and ACMS-2.5 (units: mg for pollutant, g for adsorbent and minutes for the time).

Kinetic model	Non-linear equation	Sample	q_e	k	m	*SSE*	r^2
Pseudo-first-order	$q_t = q_e \cdot (1 - \exp(-k \cdot t))$	HCMS-2.5	0.529	0.0768		0.0030	0.987
		PC	1.16	0.0401		0.180	0.864
		ACMS-2.5	1.07	0.0469		0.023	0.978
Pseudo-second-order	$q_t = \frac{1}{\frac{1}{(k \cdot q_e^2)} \cdot \frac{1}{t} + \frac{1}{(q_e)}}$	HCMS-2.5	0.553	0.270		3.1E-05	0.999
		PC	1.27	0.0430		0.079	0.940
		ACMS-2.5	1.14	0.0600		0.0036	0.997
Bangham	$q_t = k \cdot t^{1/m}$	HCMS-2.5		0.452	49.9	0.014	0.942
		PC		0.471	6.54	0.0057	0.996
		ACMS-2.5		0.537	8.68	0.038	0.963
Elovich	$q_t = \frac{1}{\beta} \cdot \ln(\alpha \cdot \beta \cdot t + 1)$	HCMS-2.5	$\alpha = 14.5$	$\beta = 21.4$		0.0063	0.975
		PC	$\alpha = 0.739$	$\beta = 6.30$		0.0061	0.995
		ACMS-2.5	$\alpha = 2.48$	$\beta = 8.27$		0.027	0.974
Dünwald-Wagner	$q_t = q_e \cdot \sqrt{1 - \exp(-k \cdot t)}$	HCMS-2.5	0.536	0.0420		0.0012	0.995
		PC	1.25	0.0135		0.097	0.929
		ACMS-2.5	1.10	0.0226		0.012	0.988
Weber-Morris	$q_t = k \cdot \sqrt{t} + m$	HCMS-2.5		0.0038	0.442	0.011	0.532
		PC		0.0203	0.714	0.035	0.910
		ACMS-2.5		0.0134	0.753	0.084	0.647
Avrami	$q_t = q_e \cdot (1 - \exp(-k \cdot t)^m)$	HCMS-2.5	0.529	0.040	1.923	0.0030	0.987
		PC	1.16	0.116	0.346	0.180	0.864
		ACMS-2.5	1.07	0.315	0.149	0.023	0.978

0.864–0.999). As expected, all models predict higher values of equilibrium adsorption capacity for PC, followed by ACMS-2.5 and HCMS-2.5.

Kinetic constants (k) for pseudo-first-order and pseudo-second-order are higher for the hydrochar (HCMS-2.5), followed by ACMS-2.5 and PC, evidencing that surface chemistry is not so determinant for the adsorption rate, as was found for the uptake capacity. The specific surface area and pore volume of the TP-based adsorbents do not show apparent relation with the kinetic constants, so the adsorption rate of Ni (II) on the ACMS-2.5, PC and HCMS-2.5 is ruled by the combination of different factors, such as textural properties and surface chemistry.

In the case of HCMS-2.5, the highest adsorption rate of Ni(II) may be ascribed to the surface chemistry and to the absence of porosity (all Ni (II) is adsorbed on its external surface, and there is no internal diffusion). The model able to better predict the kinetic adsorption of Ni(II) on HCMS-2.5 was the pseudo-second-order (q_e = 0.553 mg g^{-1}, k = 0.270 g mg^{-1} min^{-1}, r^2 = 0.999), due to the fast adsorption because of the affinity of HCMS-2.5 with Ni(II). ACMS-2.5 shows values of kinetic constant higher than PC, likely due to the highest specific surface area available (S_{ext} = 70 m^2 g^{-1} and S_{mic} = 217 m^2 g^{-1}) and moderate affinity of ACMS-2.5 according to the surface chemistry (SA = 0.78 μmol m^{-2} and SB = 2.44 μmol m^{-2}). The kinetic adsorption of Ni(II) on ACMS-2.5 was also better described by pseudo-second-order (q_e = 1.07 mg g^{-1}, k = 0.0469 g mg^{-1} min^{-1}, r^2 = 0.978).

It is typically assumed that the pseudo-second-order model fits well adsorption processes controlled by chemisorption, involving valence forces by sharing or exchange of electrons that may happen between Ni (II) and functional groups on the surface of HCMS-2.5 [58]. It is also reported that the adsorption of Ni on biomass-based adsorbents is well predicted by pseudo-second-order [50,84]. For the sample with the highest uptake capacity (PC), the pore diffusion model of Bangham was the kinetic model able to better predict the kinetic adsorption of Ni(II) on PC (k = 0.471 mg g^{-1} $min^{-1/m}$, m = 6.54, r^2 = 0.996), revealing that the process may be strongly controlled by the internal diffusion of Ni(II) inside pores of PC.

The parameter m of the kinetic model of Bangham may be used as an indicator of the intensity in the adsorption of Ni(II) [70]. In this sense, the value of 49.9 for HCMS-2.5 reveals a strong affinity for the Ni(II) on this adsorbent, as expected for the fast adsorption observed. The value is considerably higher when compared with previous works [20].

It is noteworthy that the best kinetic models predicting the adsorption of Ni(II) on each TP-based adsorbent was the same when other error functions were considered (*SAE*, *HYBRYD*, *MPSD*, and *ARE*) to fit the kinetic models, obtaining values for the parameters close to those presented minimizing *SSE*.

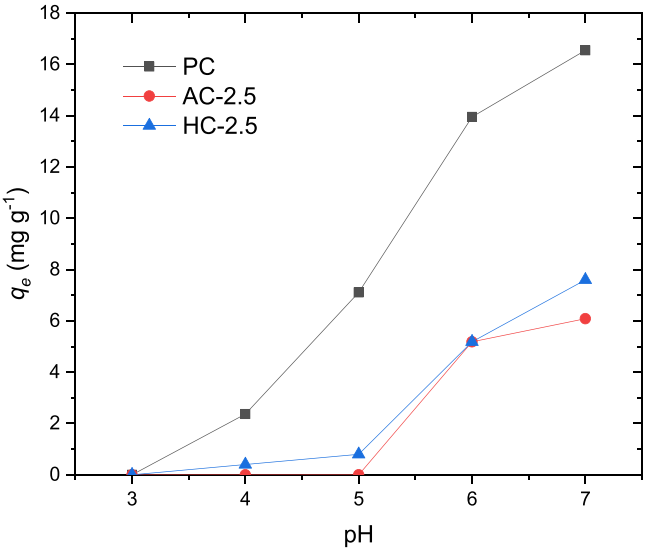

Fig. 6. Equilibria adsorption of Ni(II) on each TP-based adsorbent at different pH (Operating conditions: C_{ads} = 2.5 g L^{-1}, room temperature, and $C_{Ni\ (II),o}$ = 100 mg L^{-1}).

4.7. *Effect of pH*

In the same sense that acid-base functionalities of carbon-based adsorbents affect the adsorption of Ni(II), the pH of the aqueous solution also plays a key role in adsorption. The alteration of the pH media may cause dissociation of acid-base groups on the surface of the adsorbent and cause a significant improvement or worsening of the efficiency of removal of Ni(II) ions. In Fig. 6 is shown the effect of pH on nickel adsorption with the TP-based adsorbents evaluated.

It is notable that there is an increase in Ni adsorption at alkaline pH, as reported in literature [32,95,96]. At pH 3 there was no adsorption on any TP-based adsorbent. The adsorption of Ni is improved at a higher pH, due to the lower number of H^+ ions, while at low pH there is a competition between hydronium cations and metals, reducing the

Table 7
Maximum Ni(II) adsorption capacity (q_{max}) of different carbonaceous materials.

Carbon precursor	Adsorbent preparation	S_{BET} (m^2 g^{-1})	q_{max} (mg g^{-1})	Adsorption Conditions	Reference
Fireweed	Chemical treatment with 80 % H_2SO_4, followed by heating at 450 ºC under nitrogen flow	241	3.3	$C_{Ni(II),0}$ = 40 mg L^{-1} and C_{ads} = 0.8 g L^{-1}, 22 ºC, 18 h	Dwivedi et al., ($year $)[21]
Commercial AC (F 400)	–	–	2.8	25 ºC, pH 5	Satapathy, Natarajan ($year$)[74]
Commercial AC (F 400)	Modification with $KBrO_3$ for 1 h	–	5.8	25 ºC, pH 5	Satapathy, Natarajan ($year$)[74]
Cucumis mole peel	Carbonization in a muffle at 200 °C for 2 h.	–	5.4	$C_{Ni(II),0}$ = 100 mg L^{-1} C_{ads} = 2.5 g L^{-1}, natural pH, 25 ºC	Manjuladevi et al., ($year$)[59]
Hazelnut shell	Impregnation with concentrated H_2SO_4 and heating in a hot air oven at 150 ºC for 24 h.	441	3.9–11.6	$C_{Ni(II),0}$ = 15–200 mg L^{-1}, pH 3–8, 20–40 ºC, 3 h	(E.[22])
Phragmites australis	Treated with 85 % H_3PO_4 solution and heated to 450 °C in a muffle	1109	12.3	$C_{Ni(II),0}$ = 30 mg L^{-1}, C_{ads} = 0.6 g L^{-1}, pH 6, 25 ºC, 24 h	Yu et al., ($year$)[96]
Phenolic resin	Carbonized at 900 ºC under nitrogen stream and impregnated with Fe_2O_3	545	13.83	$C_{Ni(II),0}$ = 50 mg L^{-1}, C_{ads} = 4 g L^{-1}, pH 7, room temperature, 4 h	Lee et al., ($year$)[53]
Rice husk	Carbonized at 800 ºC for 2 h	–	4.82	$C_{Ni(II),0}$ = 150 mg L^{-1}, C_{ads} = 20 g L^{-1}, pH 6, 30 ºC, 3 h	Farhan et al., ($year$) [24]
Carbon residue from gasification process	Obtained from Woodchips at 1000 ºC	14.4	5.6	$C_{Ni(II),0}$ = 25 mg L^{-1}, C_{ads} = 5 g L^{-1}, pH 8, room temperature, 24 h	Runtti et al., ($year$) [72]
Chemically ($ZnCl_2$) AC residue	–	254	18.2	$C_{Ni(II),0}$ = 125 mg L^{-1}, C_{ads} = 5 g L^{-1}, pH 8, room temperature, 24 h	Runtti et al., ($year$) [72]
Commercial AC	–	603	2.9	$C_{Ni(II),0}$ = 25 mg L^{-1}, C_{ads} = 5 g L^{-1}, pH 8, room temperature, 24 h	Runtti et al., ($year$) [72]
Tangerine peels	Carbonization at 800 ºC for 4 h (PC sample)	104	16.5	$C_{Ni(II),0}$ = 100 mg L^{-1}, C_{ads} = 2.5 g L^{-1}, pH 8, room temperature, 72 h	This study
Tangerine peels	HTC with $FeCl_3$ 2.5 M at 200 ºC for 3 h (HCMS-2.5 sample)	11	7.6	$C_{Ni(II),0}$ = 100 mg L^{-1}, C_{ads} = 2.5 g L^{-1}, pH 8, room temperature, 72 h	This study
Tangerine peels	Carbonization at 800 ºC for 4 h (PC sample)	104	1.99	$C_{Ni(II),0}$ = 5 mg L^{-1}, C_{ads} = 2.5 g L^{-1}, pH 6, room temperature, 72 h	This study
Tangerine peels	HTC with $FeCl_3$ 2.5 M at 200 ºC for 3 h (HCMS-2.5 sample)	11	0.60	$C_{Ni(II),0}$ = 5 mg L^{-1}, C_{ads} = 2.5 g L^{-1}, pH 6, room temperature, 72 h	This study

adsorption of metal ions [1,57]. When the pH is higher, the concentration of H_3O^+ ions decreases and the sites on the surface of the carbon turn mainly into dissociated forms and can exchange H_3O^+ ions with metal ions in solution [86].

4.8. Ni(II) adsorption mechanism and capacity

According to the above results related to the characterization of the TP-based adsorbents and their performance, it can be concluded that textural properties and mainly surface chemistry plays a significant role in Ni(II) adsorption. HCMS-2.5 adsorbent shows a significant uptake capacity of Ni taking into account its BET surface (11 m^2 g^{-1}), reaching the highest Ni adsorption capacity per surface area (54.6 μg m^{-2}). FT-IR and XPS spectra revealed that HCMS-2.5 is rich in SOGs mainly consisting of hydroxyl groups. PC sample, which was prepared by pyrolysis of the raw precursor at higher temperatures than HCMS-2.5, also presents a significant content of oxygen on its surface. Its functionalization, coupled with a higher porosity, make it a standout adsorbent for Ni removal. The pyrolysis of HCMS-2.5 to obtain ACMS-2.5 results in activated carbon microspheres with the highest surface area, but the adsorbent does not display a surface chemistry suitable for adsorption of Ni. A proper combination of SOGs allows adsorbing Ni by cation exchange (hydroxyl and carboxylic groups), electrostatic attraction (ester, carbonyl groups) or complexation (epoxy, ether groups) [37,96]. Taking into account that pseudo-second order model is the best kinetic model able to predict Ni adsorption on these adsorbents, it is expected that the process is controlled by chemisorption, involving valence forces by sharing or exchange of electrons because of the functional groups on their surface.

Table 7 gives a comparison of the maximum Ni(II) adsorption capacity on different carbonaceous materials reported in literature. As observed, TP-based adsorbents show values of uptake capacity similar or higher than others reported taking into account the diverse operating conditions in the adsorption of Ni(II) found in literature ($C_{Ni(II),0}$ = 30–150 mg L^{-1}, C_{ads} = 0.6–20 g L^{-1}, 20–40 ºC, pH 3–8, 3–24 h of contact time).

5. Conclusions

The successful preparation of hydrochar and activated carbon microspheres from tangerine peels has been proved by hydrothermal carbonization with $FeCl_3$ followed by pyrolysis at mild and moderate conditions, respectively, evidencing that biomass waste, such as citrus fruit peels, may be turned into high-added value materials in the context of a circular economy approach. The presence of chemical agents, such as $FeCl_3$ in hydrothermal carbonization, has resulted in an effective tool for tuning the morphology, surface chemistry and increased carbonization yields in hydrochars and further preparation of activated carbons from those hydrochars. Furthermore, it was demonstrated that the shape and size of the microspheres obtained by hydrothermal carbonization are maintained even after heating to obtain activated carbon microspheres with higher porosity.

The role played by textural properties and surface chemistry of carbonaceous adsorbents has been elucidated, concluding that the functionality of carbon-based materials is determinant in their performance for the adsorption of Ni (the highest uptake capacity of Ni was found with pyrochar, which shows a basicity of 1.83 mmol g^{-1} and a S_{BET} of 104 m^2 g^{-1}, whereas a poor adsorption capacity was observed with the activated carbon, which has a S_{BET} of 287 m^2 g^{-1}).

The best isotherm and kinetic models predicting the adsorption of Ni on the carbonaceous materials were different among them due to their unique characteristics. Langmuir, Khan, and Jovanović are models that best represent the adsorption of Ni on the activated carbon, pyrochar and hydrochar, respectively. On the other hand, kinetic adsorption of Ni was well predicted by the pseudo-second order model for activated carbon and hydrochar. In contrast, the adsorption of Ni on pyrochar was represented by the Bangham model.

CRediT authorship contribution statement

Jose L. Diaz de Tuesta: Investigation, Conceptualization, Methodology, Formal analysis, Writing – original draft preparation, Visualization. **Fernanda F. Roman**: Investigation, Validation. **Vitor C. Marques**: Investigation, Writing – original draft preparation. **Adriano S. Silva**: Investigation. **Ana P.F. Silva**: Investigation. **Assem A. Shinibekova**: Investigation. **Sadenova Aknur**: Investigation. **Marzhan S. Kalmakhanova**: Supervision. **Bakytgul K. Massalimova**: Supervision. **Margarida Arrobas**: Investigation. **Tatiane C. Bosco**: Supervision. **Adrián M.T. Silva**: Supervision, Writing – review & editing, Funding acquisition, Project administration. **Helder T. Gomes**: Supervision, Conceptualization, Writing – reviewing & editing, Funding acquisition, Project administration.

Declaration of Competing Interest

The authors declare the following financial interests/personal relationships which may be considered as potential competing interests: Helder Teixeira Gomes reports financial support was provided by European Regional Development.

Acknowledgments

The authors are grateful to the FCT (Foundation for Science and Technology, Portugal) and FEDER (European Regional Development Fund) under Programme PT2020 for financial support to CIMO (UIDB/00690/2020). We would also like to thank the scientific collaboration under Base-UIDB/50020/2020 and Programmatic-UIDP/50020/2020 funding of LSRE-LCM, and LA/P/0045/2020 funding of ALiCE, funded by national funds through FCT and MCTES (Ministério da Ciência, Tecnologia e Ensino Superior, Portugal) by PIDDAC (Programa de Investimentos e Despesas de Desenvolvimento da Administração Central, Portugal). Fernanda F. Roman and Adriano dos Santos Silva acknowledge the national funding by FCT and MIT (Massachusetts Institute of Technology, USA), and the ESF (European Social Fund) for individual research grants with reference numbers of SFRH/BD/143224/2019 and SFRH/BD/151346/2021, respectively.

Appendix A. Supporting information

Supplementary data associated with this article can be found in the online version at doi:10.1016/j.jece.2022.108143.

References

[1] S. Afroze, T.K. Sen, A review on heavy metal ions and dye adsorption from water by agricultural solid waste adsorbents, Water Air Soil Pollut. 229 (2018) 225.
[2] M.J. Ahmed, Application of agricultural based activated carbons by microwave and conventional activations for basic dye adsorption: review, J. Environ. Chem. Eng. 4 (2016) 89–99.
[3] J. Alcañiz-Monge, M.Á. Lillo-Ródenas, A. Bueno-López, M.J. Illán-Gómez, The influence of iron chloride addition to the precursor pitch on the formation of activated carbon fibers, Micro Mesop. Mater. 100 (2007) 202–209.
[4] P.J. Arauzo, M.P. Olszewski, X. Wang, J. Pfersich, V. Sebastian, J. Manyà, N. Hedin, A. Kruse, Assessment of the effects of process water recirculation on the surface chemistry and morphology of hydrochar, Renew. Energy 155 (2020) 1173–1180.
[5] P. Bartczak, M. Norman, Ł. Klapiszewski, N. Karwańska, M. Kawalec, M. Baczyńska, M. Wysokowski, J. Zdarta, F. Ciesielczyk, T. Jesionowski, Removal of nickel(II) and lead(II) ions from aqueous solution using peat as a low-cost adsorbent: a kinetic and equilibrium study, Arab. J. Chem. 11 (2018) 1209–1222.
[6] I. Bautista-Toledo, M.A. Ferro-García, J. Rivera-Utrilla, C. Moreno-Castilla, F. J. Vegas Fernández, Bisphenol A removal from water by activated carbon. Effects of carbon characteristics and solution chemistry, Environ. Sci. Technol. 39 (2005) 6246–6250.
[7] H.P. Boehm, Some aspects of the surface chemistry of carbon blacks and other carbons, Carbon 32 (1994) 759–769.
[8] F. Brouers, O. Sotolongo, F. Marquez, J.P. Pirard, Microporous and heterogeneous surface adsorption isotherms arising from Levy distributions, Phys. A 349 (2005) 271–282.
[9] H. Cai, X. Lin, L. Tian, X. Luo, One-step hydrothermal synthesis of carbonaceous spheres from glucose with an aluminum chloride catalyst and its adsorption characteristic for uranium(VI), Ind. Eng. Chem. Res. 55 (2016) 9648–9656.
[10] M. Cempel, G. Nikel, Nickel: A review of its sources and environmental toxicology, Pol. J. Environ. Stud. 15 (2006) 375–382.
[11] Q. Chang, W. Lin, W.C. Ying, Preparation of iron-impregnated granular activated carbon for arsenic removal from drinking water, J. Hazard. Mater. 184 (2010) 515–522.
[12] G. Chattopadhyaya, D.G. Macdonald, N.N. Bakhshi, J.S. Soltan Mohammadzadeh, A.K. Dalai, Preparation and characterization of chars and activated carbons from Saskatchewan lignite, Fuel Process. Technol. 87 (2006) 997–1006.
[13] A. a M. Daifullah, B.S. Girgis, H.M.H. Gad, Utilization of agro-residues (rice husk) in small waste water treatment plans, Mater. Lett. 57 (2003) 1723–1731.
[14] W.M. Daud, W.S. Ali, Comparison on pore development of activated carbon produced from palm shell and coconut shell, Bioresour. Technol. 93 (2004) 63–69.
[15] G. De Freitas Batista, F.F. Roman, J.L.D. De Tuesta, R.V. Mambrini, P. Praça, H. T. Gomes, Assessment of pretreatments for highly concentrated leachate waters to enhance the performance of catalytic wet peroxide oxidation with sustainable low-cost catalysts, Catalysts 12 (2022) 238.
[16] J.L. Diaz De Tuesta, M. C. Saviotti, F. F. Roman, G. F. Pantuzza, H. J.F. Sartori, A. Shinibekova, M. S. Kalmakhanova, B. K. Massalimova, J. M.T.A. Pietrobelli, G. G. Lenzi, H. T. Gomes, Assisted hydrothermal carbonization of agroindustrial byproducts as effective step in the production of activated carbon catalysts for wet peroxide oxidation of micro-pollutants, J. Environ. Chem. Eng. 9 (2021), 105004.
[17] J.L. Diaz De Tuesta, F.V.M. De Almeida, J.R.P. Oliveira, P. Praça, M.C. Guerreiro, H.T. Gomes, Kinetic insights on wet peroxide oxidation of caffeine using EDTA-functionalized low-cost catalysts prepared from compost generated in municipal solid waste treatment facilities, Environ. Tech. Inno. 24 (2021), 101984.
[18] J.L. Diaz De Tuesta, G. F. Pantuzza, A. M. T. Silva, P. Praça, J.L. Faria, H.T. Gomes, Catalysts prepared with matured compost derived from mechanical-biological treatment plants for the wet peroxide oxidation of pollutants with different lipophilicity, Catalysts 10 (2020) 1243.
[19] J.L. Diaz De Tuesta, A.M.T. Silva, J.L. Faria, H.T. Gomes, Removal of Sudan IV from a simulated biphasic oily wastewater by using lipophilic carbon adsorbents, Chem. Eng. J. 347 (2018) 963–971.
[20] J.L. Diaz De Tuesta, A.M.T. Silva, J.L. Faria, H.T. Gomes, Adsorption of Sudan-IV contained in oily wastewater on lipophilic activated carbons: kinetic and isotherm modelling, Environ. Sci. Pollut. Res. 27 (2020) 20770–20785.
[21] A.D. Dwivedi, S.P. Dubey, M. Sillanpää, Y.-N. Kwon, C. Lee, Distinct adsorption enhancement of bi-component metals (cobalt and nickel) by Fireweed-derived carbon compared to activated carbon: incorporation of surface group distributions for increased efficiency, Chem. Eng. J. 281 (2015) 713–723.
[22] E. Demirbas, M. Kobya, S. Oncel, S. Sencan, Removal of Ni(II) from aqueous solution by adsorption onto hazelnut shell activated carbon: equilibrium studies, Bioresour. Technol. 84 (2002) 291–293.
[23] E. Erdogan, B. Atila, J. Mumme, M.T. Reza, A. Toptas, M. Elibol, J. Yanik, Characterization of products from hydrothermal carbonization of orange pomace including anaerobic digestibility of process liquor, Bioresour. Technol. 196 (2015) 35–42.
[24] A.T.A. Farhan, K.K. Ong, W.M.Z.W. Yunus, M.L. Jabit, A. Fitrianto, U.F.A. Rauf, A. G. Hussin, C.C. Teoh, M.B. Ahmad, Optimisation of nickel (II) adsorption using thermally treated rice husk, Int. J. Appl. Environ. Sci. 11 (2016) 717–730.
[25] M.E. Fernandez, B. Ledesma, S. Roman, P.R. Bonelli, A.L. Cukierman, Development and characterization of activated hydrochars from orange peels as potential adsorbents for emerging organic contaminants, Bioresour. Technol. 183 (2015) 221–228.
[26] M.E. Fernandez, G.V. Nunell, P.R. Bonelli, A.L. Cukierman, Activated carbon developed from orange peels: batch and dynamic competitive adsorption of basic dyes, Ind. Crops Prod. 62 (2014) 437–445.
[27] V. Fierro, G. Muniz, G. Gonzalez-Sanchez, M.L. Ballinas, A. Celzard, Arsenic removal by iron-doped activated carbons prepared by ferric chloride forced hydrolysis, J. Hazard. Mater. 168 (2009) 430–437.
[28] K.Y. Foo, B.H. Hameed, Insights into the modeling of adsorption isotherm systems, Chem. Eng. J. 156 (2010) 2–10.
[29] C.H. Giles, D. Smith, A. Huitson, A general treatment and classification of the solute adsorption isotherm. I. Theoretical, J. Colloid Interface Sci. 47 (1974) 755–765.
[30] M.L. Godino-Salido, R. López-Garzón, M.D. Gutiérrez-Valero, P. Arranz-Mascarós, M. Melguizo-Guijarro, M.D. López De La Torre, V. Gómez-Serrano, M. Alexandre-Franco, D. Lozano-Castelló, D. Cazorla-Amorós, M. Domingo-García, Effect of the surface chemical groups of activated carbons on their surface adsorptivity to aromatic adsorbates based on π-π interactions, Mater. Chem. Phys. 143 (2014) 1489–1499.
[31] J. Guo, B. Gui, S.-X. Xiang, X.-T. Bao, H.-J. Zhang, A.C. Lua, Preparation of activated carbons by utilizing solid wastes from palm oil processing mills, J. Porous Mater. 15 (2007) 535–540.
[32] Z. Guo, J. Zhang, H. Liu, Y. Kang, J. Yu, C. Zhang, Optimization of the green and low-cost ammoniation-activation method to produce biomass-based activated carbon for Ni(II) removal from aqueous solutions, J. Clean. Prod. 159 (2017) 38–46.
[33] A. Gurses, C. Dogar, M. Yalcin, M. Acikyildiz, R. Bayrak, S. Karaca, The adsorption kinetics of the cationic dye, methylene blue, onto clay, J. Hazard. Mater. 131 (2006) 217–228.
[34] C. Hinz, Description of sorption data with isotherm equations, Geoderma 99 (2001) 225–243.

[35] B. Hu, K. Wang, L. Wu, S.H. Yu, M. Antonietti, M.M. Titirici, Engineering carbon materials from the hydrothermal carbonization process of biomass, Adv. Mater. 22 (2010) 813–828.
[36] B. Hu, S.-H. Yu, K. Wang, L. Liu, X.-W. Xu, Functional carbonaceous materials from hydrothermal carbonization of biomass: an effective chemical process, Dalton Trans. (2008) 5414–5423.
[37] M.A. Islam, M.R. Awual, M.J. Angove, A review on nickel(II) adsorption in single and binary component systems and future path, J. Environ. Chem. Eng. 7 (2019), 103305.
[38] L. Izquierdo, J.M. Sendra, CITRUS FRUITS | Composition and Characterization, in: B. Caballero (Ed.), Encyclopedia of Food Sciences and Nutrition, Second edition.,, Academic Press, Oxford, 2003.
[39] M. Jain, V.K. Garg, K. Kadirvelu, Removal of Ni(II) from aqueous system by chemically modified sunflower biomass, Desalin. Water Treat. 52 (2014) 5681–5695.
[40] W. Jiang, L. Zhang, X. Guo, M. Yang, Y. Lu, Y. Wang, Y. Zheng, G. Wei, Adsorption of cationic dye from water using an iron oxide/activated carbon magnetic composites prepared from sugarcane bagasse by microwave method, Environ. Technol. (2019) 1–14.
[41] D.S. Jovanović, Physical adsorption of gases, Kolloid-Z. und Z. für Polym. 235 (1969) 1203–1213.
[42] R.R. Karri, J.N. Sahu, N.S. Jayakumar, Optimal isotherm parameters for phenol adsorption from aqueous solutions onto coconut shell based activated carbon: Error analysis of linear and non-linear methods, J. Taiwan Inst. Chem. E. 80 (2017) 472–487.
[43] A.R. Khan, T.A. Al-Bahri, A. Al-Haddad, Adsorption of phenol based organic pollutants on activated carbon from multi-component dilute aqueous solutions, Water Res. 31 (1997) 2102–2112.
[44] A.R. Khan, I.R. Al-Waheab, A. Al-Haddad, A generalized equation for adsorption isotherms for multi-component organic pollutants in dilute aqueous solution, Environ. Technol. 17 (1996) 13–23.
[45] A.R. Khan, R. Ataullah, A. Al-Haddad, Equilibrium adsorption studies of some aromatic pollutants from dilute aqueous solutions on activated carbon at different temperatures, J. Colloid Interface Sci. 194 (1997) 154–165.
[46] R.A. Koble, T.E. Corrigan, Adsorption isotherms for pure hydrocarbons, Ind. Eng. Chem. 44 (1952) 383–387.
[47] K.V. Kumar, K. Porkodi, Relation between some two- and three-parameter isotherm models for the sorption of methylene blue onto lemon peel, J. Hazard. Mater. 138 (2006) 633–635.
[48] K.V. Kumar, K. Porkodi, F. Rocha, Isotherms and thermodynamics by linear and non-linear regression analysis for the sorption of methylene blue onto activated carbon: comparison of various error functions, J. Hazard. Mater. 151 (2008) 794–804.
[49] K.V. Kumar, S. Sivanesan, Pseudo second order kinetic models for safranin onto rice husk: comparison of linear and non-linear regression analysis, Process Biochem. 41 (2006) 1198–1202.
[50] P.S. Kumar, S. Ramalingam, S.D. Kirupha, A. Murugesan, T. Vidhyadevi, S. Sivanesan, Adsorption behavior of nickel(II) onto cashew nut shell: equilibrium, thermodynamics, kinetics, mechanism and process design, Chem. Eng. J. 167 (2011) 122–131.
[51] S. Kumar, A.V. Trivedi, A review on role of nickel in the biological system, Int. J. Curr. Microbiol. Appl. Sci. 5 (2016) 719–727.
[52] I. Langmuir, The adsorption of gases on plane surfaces of glass, mica and platinum, J. Am. Chem. Soc. 40 (1918) 1361–1403.
[53] C.G. Lee, S. Lee, J.A. Park, C. Park, S.J. Lee, S.B. Kim, B. An, S.T. Yun, S.H. Lee, J. W. Choi, Removal of copper, nickel and chromium mixtures from metal plating wastewater by adsorption with modified carbon foam, Chemosphere 166 (2017) 203–211.
[54] J. Lin, L. Wang, Comparison between linear and non-linear forms of pseudo-first-order and pseudo-second-order adsorption kinetic models for the removal of methylene blue by activated carbon, Front. Environ. Sci. Eng. China 3 (2009) 320–324.
[55] D. Liu, B. Jia, X. Liu, B. Zhao, J. Gao, Q. Cao, S. Wu, Y. Qin, Effects of oxygen functional groups and FeCl3 on the evolution of physico-chemical structure in activated carbon obtained from Jixi bituminous coal, RSC Adv. 8 (2018) 8569–8579.
[56] E.C.N. Lopes, F.S.C. Dos Anjos, E.F.S. Vieira, A.R. Cestari, An alternative Avrami equation to evaluate kinetic parameters of the interaction of Hg(II) with thin chitosan membranes, J. Colloid Interface Sci. 263 (2003) 542–547.
[57] Z. Mahdi, Q.J. Yu, A. El Hanandeh, Competitive adsorption of heavy metal ions (Pb2+, Cu2+, and Ni2+) onto date seed biochar: batch and fixed bed experiments, Sep. Sci. Technol. 54 (2018) 888–901.
[58] G.F. Malash, M.I. El-Khaiary, Methylene blue adsorption by the waste of Abu-Tartour phosphate rock, J. Colloid Interface Sci. 348 (2010) 537–545.
[59] M. Manjuladevi, R. Anitha, S. Manonmani, Kinetic study on adsorption of Cr(VI), Ni(II), Cd(II) and Pb(II) ions from aqueous solutions using activated carbon prepared from Cucumis melo peel, Appl. Water Sci. 8 (2018).
[60] S.E. Mansour, I.H. Hasieb, Removal of nickel from drinking water by electrocoagulation technique using alternating current, Curr. Res. Chem. 4 (2012) 41–50.
[62] W. Mertz, The essential trace elements, Science 213 (1981) 1332–1338.
[63] K. Mohsen, J.L. Diaz De Tuesta, C.N.D.P. Gonçalves, H.T. Gomes, A.E. Rodrigues, A.C.S. José, Integrated management of environment by employing derived compost from municipal solid wastes as a source of biochar for CO_2 capture, Chem. Eng. Technol. 43 (2020) 1336–1349.
[64] P. Mondal, C. Balo Majumder, B. Mohanty, Removal of trivalent arsenic (As(III)) from contaminated water by calcium chloride (CaCl2)-impregnated rice husk carbon, Ind. Eng. Chem. Res. 46 (2007) 2550–2557.
[65] Poonam, N. Kumar, Experimental and kinetic study of removal of lead (Pb+2) from battery effluent using sweet lemon (Citrus limetta) peel biochar adsorbent, Environ. Dev. Sustain. 22 (2019) 4379–4406.
[66] F. Quesada-Plata, R. Ruiz-Rosas, E. Morallón, D. Cazorla-Amorós, Activated carbons prepared through H_3PO_4-assisted hydrothermal carbonisation from biomass wastes: porous texture and electrochemical performance, ChemPlusChem 81 (2016) 1349–1359.
[67] C.J. Radke, J.M. Prausnitz, Adsorption of organic solutes from dilute aqueous solution of activated carbon, Ind. Eng. Chem. Fundam. 11 (1972) 445–451.
[68] O. Redlich, D.L. Peterson, A useful adsorption isotherm, J. Phys. Chem. 63 (1959), 1024-1024.
[69] N.G. Rincón-Silva, J.C. Moreno-Piraján, L. Giraldo, Equilibrium, kinetics and thermodynamics study of phenols adsorption onto activated carbon obtained from lignocellulosic material (Eucalyptus globulus labill seed), Adsorpt 22 (2015) 33–48.
[70] A. Rodriguez, J. Garcia, G. Ovejero, M. Mestanza, Adsorption of anionic and cationic dyes on activated carbon from aqueous solutions: equilibrium and kinetics, J. Hazard. Mater. 172 (2009) 1311–1320.
[71] F.F. Roman, J.L. Diaz De Tuesta, P. Praça, A.M.T. Silva, J.L. Faria, H.T. Gomes, Hydrochars from compost derived from municipal solid waste: production process optimization and catalytic applications, J. Environ. Chem. Eng. 9 (2021), 104888.
[72] H. Runtti, S. Tuomikoski, T. Kangas, U. Lassi, T. Kuokkanen, J. Rämö, Chemically activated carbon residue from biomass gasification as a sorbent for iron(II), copper (II) and nickel(II) ions, J. Water Process Eng. 4 (2014) 12–24.
[73] A. Santos Silva, M. Seitovna Kalmakhanova, B. Kabykenovna Massalimova, J. G. Sgorlon, J.L. Diaz De Tuesta, H. T. Gomes, Wet peroxide oxidation of paracetamol using acid activated and Fe/Co-pillared clay catalysts prepared from natural clays, Catalysts 9 (2019) 705.
[74] D. Satapathy, G.S. Natarajan, Potassium bromate modification of the granular activated carbon and its effect on nickel adsorption, Adsorpt 12 (2006) 147–154.
[75] B. Satari, K. Karimi, Citrus processing wastes: environmental impacts, recent advances, and future perspectives in total valorization, Resour., Conserv. Recycl. 129 (2018) 153–167.
[76] J.Z. Savić, V.M. Vasić, Thermodynamics and kinetics of 1,8-dihydroxy-2-(imidazol-5-ylazo)-naphthalene-3,6-disulphonic acid immobilization on Dowex resin, Colloids Surf. A 278 (2006) 197–203.
[77] P. Senthil Kumar, S. Ramalingam, C. Senthamarai, M. Niranjanaa, P. Vijayalakshmi, S. Sivanesan, Adsorption of dye from aqueous solution by cashew nut shell: Studies on equilibrium isotherm, kinetics and thermodynamics of interactions, Desalination 261 (2010) 52–60.
[78] A. Shakya, A. Nunez-Delgado, T. Agarwal, Biochar synthesis from sweet lime peel for hexavalent chromium remediation from aqueous solution, J. Environ. Manag. 251 (2019), 109570.
[79] K. Sharma, N. Mahato, M.H. Cho, Y.R. Lee, Converting citrus wastes into value-added products: economic and environmently friendly approaches, Nutrition 34 (2017) 29–46.
[80] R.M. Shrestha, M. Varga, I. Varga, A.P. Yadav, B.P. Pokharel, R.R. Pradhananga, Removal of Ni (II) from aqueous solution by adsorption onto activated carbon prepared from lapsi (Choerospondias axillaris) seed stone, J. Inst. Eng. 9 (2014) 166–174.
[81] A. Siddique, A.K. Nayak, J. Singh, Synthesis of FeCl3-activated carbon derived from waste Citrus limetta peels for removal of fluoride: an eco-friendly approach for the treatment of groundwater and bio-waste collectively, Groundw. Sustain. Dev. 10 (2020), 100339.
[82] R. Sips, On the structure of a catalyst surface, J. Chem. Phys. 16 (1948) 490–495.
[83] C. Son, W. An, G. Lee, I. Jeong, Y.-G. Lee, K. Chon, Adsorption characteristics of phosphate ions by pristine, CaCl2 and FeCl3-activated biochars originated from tangerine peels, Separations 8 (2021) 32.
[84] R. Sudha, K. Srinivasan, P. Premkumar, Kinetic, mechanism and equilibrium studies on removal of Pb(II) using Citrus limettioides peel and seed carbon, Res. Chem. Intermed. 42 (2015) 1677–1697.
[85] R.F. Susanti, A.A. Arie, H. Kristianto, M. Erico, G. Kevin, H. Devianto, Activated carbon from citric acid catalyzed hydrothermal carbonization and chemical activation of salacca peel as potential electrode for lithium ion capacitor's cathode, Ionics 25 (2019) 3915–3925.
[86] V.C. Taty-Costodes, H. Fauduet, C. Porte, A. Delacroix, Removal of Cd(II) and Pb (II) ions, from aqueous solutions, by adsorption onto sawdust of Pinus sylvestris, J. Hazard. Mater. 105 (2003) 121–142.
[87] M.M. Titirici, A. Thomas, Yu Shu-Hong, J.-O. Müller, M. Antonietti, A direct synthesis of mesoporous carbons with bicontinuous pore morphology from crude plant material by hydrothermal carbonization, Chem. Mater. 19 (2007) 4205–4212.
[88] J. Tóth, A uniform interpretation of gas/solid adsorption, J. Colloid Interface Sci. 79 (1981) 85–95.
[89] H.N. Tran, S.-J. You, H.-P. Chao, Effect of pyrolysis temperatures and times on the adsorption of cadmium onto orange peel derived biochar, Waste Manag. Res. 34 (2016) 129–138.
[90] V. Tucureanu, A. Matei, A.M. Avram, FTIR spectroscopy for carbon family study, Crit. Rev. Anal. Chem. 46 (2016) 502–520.
[91] A.M.M. Vargas, A.L. Cazetta, M.H. Kunita, T.L. Silva, V.C. Almeida, Adsorption of methylene blue on activated carbon produced from flamboyant pods (Delonix regia): study of adsorption isotherms and kinetic models, Chem. Eng. J. 168 (2011) 722–730.

[92] W.R. Vieth, K.J. Sladek, A model for diffusion in a glassy polymer, J. Colloid Sci. 20 (1965) 1014–1033.
[93] L. Wang, Application of activated carbon derived from 'waste' bamboo culms for the adsorption of azo disperse dye: kinetic, equilibrium and thermodynamic studies, J. Environ. Manag. 102 (2012) 79–87.
[94] M.A. Yahya, Z. Al-Qodah, C.W.Z. Ngah, Agricultural bio-waste materials as potential sustainable precursors used for activated carbon production: a review, Renew. Sust. Energ. Rev. 46 (2015) 218–235.
[95] W. Yin, C. Zhao, J. Xu, J. Zhang, Z. Guo, Y. Shao, Removal of Cd(II) and Ni(II) from aqueous solutions using activated carbon developed from powder-hydrolyzed-feathers and Trapa natans husks, Colloids Surf. A 560 (2019) 426–433.
[96] J. Yu, J. Zhang, S. Song, H. Liu, Z. Guo, C. Zhang, Removal of Ni(II) from aqueous solutions using activated carbon with manganese formate hydrate in-situ modification, Colloids Surf. A 560 (2019) 84–91.
[97] Z. Zhang, Z. Zhu, B. Shen, L. Liu, Insights into biochar and hydrochar production and applications: a review, Energy 171 (2019) 581–598.
[98] J. Zhao, X. Shi, V. Castranova, M. Ding, Occup. Toxicol. Nickel Nickel Compd. 28 (2009) 177–208.